

Contents lists available at ScienceDirect

Petroleum Science





Original Paper

Natural fractures controlled by strike-slip faults in ultradeep carbonate reservoirs: A case study of the Middle and Lower Ordovician in the Tarim Basin, China



Dong-Sheng Cao ^{a,b,c,d,e}, Jun Han ^f, Lian-Bo Zeng ^{a,b,g,*}, Cheng Huang ^f, Paul Dirk Bons ^{e,h}, Guo-Ping Liu ^{g,h}, Ying-Tao Yao ^{a,b}, Zhe Mao ^{a,b}, Wen-Ya Lyu ^{a,b}, Isaac Naaman ^e, Ling-Ping Zeng ⁱ

- ^a State Key Laboratory of Petroleum Resource and Prospecting, China University of Petroleum (Beijing), Beijing, 102249, China
- ^b College of Geoscience, China University of Petroleum (Beijing), Beijing, 102249, China
- ^c State Key Laboratory of Continental Shale Oil, Northeast Petroleum University, Daqing, 163318, Heilongjiang, China
- ^d School of Earth Sciences, Northeast Petroleum University, Daqing, 163318, Heilongjiang, China
- e Department of Geosciences, Eberhard Karls University of Tübingen, Schnarrenbergstr. 94–96, Tübingen, 72076, Baden-Württemberg, Germany
- f Research Institute of Petroleum Exploration and Production, SINOPEC Northwest Company, Urumqi, 830011, Xinjiang, China
- g Institute of Energy, Peking University, Beijing, 100871, China
- h School of Earth Science and Resources, China University of Geosciences, Beijing, 100083, China
- ¹ CSIRO Energy, 71 Normanby Road, Clayton North, Monash, Victoria, 3169, Australia

ARTICLE INFO

Article history: Received 2 July 2023 Received in revised form 11 November 2024 Accepted 19 May 2025 Available online 20 May 2025

Edited by Teng Zhu

Keywords: Ultradeep carbonate reservoirs Strike-slip fault Natural fractures Fault stepover Tarim Basin

ABSTRACT

Natural fractures controlled by faults in ultradeep carbonate strata play substantial roles as both fluid migration channels and storage spaces. However, characterizing the heterogeneous distribution of underground fractures within the complex three-dimensional geometry of strike-slip fault zones remains challenging. This study investigates the characteristics of natural fractures controlled by strikeslip faults in the fractured Middle and Lower Ordovician reservoirs of the central and northern Tarim Basin, China, Seismics, cores, and image logs were integrated to quantitatively analyze the intensity and dip angle of natural fractures and findings were verified using published sandbox simulations. The carbonate reservoir contains three main types of natural fractures: tectonic fractures, abnormal highpressure-related fractures, and stylolites. Strike-slip faults control the distribution and characteristics of tectonic fractures across various scales. Generally, both fracture intensity and porosity exhibit a decreasing trend as the distance from the main fault surface increases. Compared with those in nonstepover zones along a strike-slip fault, natural fractures and faults in stepover zones are more developed along the fault strike, with significantly greater development intensity in central stepover regions than that at its two ends. Furthermore, strike-slip faults influence the dip angles of both natural fractures and secondary faults. The proportion of medium-to-low-dip angle fractures and faults in the stepover zone is greater than that in the non-stepover zone. Additionally, the proportion of medium-to low-dip angle fractures and faults in the middle of the stepover is greater than that at both ends. Therefore, strike-slip fault structures control the dip angle of natural fracture and the heterogeneity of secondary fault and fracture intensity. The linking damage zone in the stepover contains a larger volume of fractured rocks, making it a promising petroleum exploration target. The development of stepovers and the orientation of present-day in-situ stress substantially influence the productivity of fractured reservoirs controlled by strike-slip faults. The analysis in this study reveals that reservoir productivity increases as the angle between the strike-slip fault segment and the maximum horizontal principal stress decreases. This study provides valuable insights for quantitatively evaluating fracture heterogeneity in fractured reservoirs and establishing optimized selection criteria for favorable targets in faultrelated fractured reservoirs.

© 2025 The Authors. Publishing services by Elsevier B.V. on behalf of KeAi Communications Co. Ltd. This is an open access article under the CC BY-NC-ND license (http://creativecommons.org/licenses/by-nc-nd/4.0/).

E-mail address: lbzeng@sina.com (L.-B. Zeng).

^{*} Corresponding author.

1. Introduction

Carbonate reservoirs play a substantial role in the global petroleum industry, accounting for over 60% and 40% of global oil and gas reserves, respectively (Agosta and Tondi, 2010), Most carbonate reservoirs are considered naturally fractured or fault- and fracture-related karst reservoirs (Wennberg et al., 2016; Zeng et al., 2024a). These fractured carbonate formations serve as critical reservoirs for various subsurface resources, including groundwater, oil and gas, or geothermal energy (van Der Voet et al., 2020). Fractures affect the permeability and porosity of rocks and the performance of reservoirs (Hennings et al., 2012; Wu et al., 2020; Wang et al., 2023). This is particularly relevant to deep or ultradeep reservoirs with a depth >6000 m (Wang et al., 2020; Zhang et al., 2023), given that the original rock porosity typically decreases with increasing depth (Ingebritsen and Manning, 1999). However, (ultra) deep carbonate reservoirs have now been recognized as important targets for oil and gas exploration (He et al., 2016; Ma et al., 2022; Zeng et al., 2023a; Laubach et al., 2023). Previous studies on carbonate reservoirs have primarily focused on sequence stratigraphy and sedimentary facies (Yang et al., 2010), karst paleogeomorphology (Zeng et al., 2023a), diagenetic evolution (Zhou et al., 2020; Liu et al., 2020a), discrete fracture network modeling (Yao et al., 2024), structural styles and genetic mechanisms of faults (Yang et al., 2014a, 2014b, 2021a; Wu et al., 2021; Jia et al., 2022), and associated petroleum migration and preservation processes (Pang et al., 2010; Su et al., 2017; Smeraglia et al., 2022a, 2022b). However, research on natural fracture systems in ultradeep carbonate reservoirs remains relatively limited. Therefore, it is of vital importance and urgency to understand the development and characteristics of natural fractures in deep carbonate reservoirs.

The development of fractures in layered sedimentary rocks is governed by multiple controlling factors, which include (1) local to regional tectonic (faults, folds, etc.) and stress regime, (2) lithostratigraphic setting, (3) hydrogeological architecture, (4) diagenetic processes, (5) driving deformation mechanisms (e.g., structural bending vs. hydrofracturing), and (6) intrinsic mechanical properties of lithological units and their coupling at interfaces (Ogata et al., 2017 and reference therein). A fault can be divided into damage zones and a fault core, which controls the development characteristics of fractures (Caine et al., 1996; Faulkner et al., 2010). Fracture density exhibits a gradual decrease as the distance from the fault core increases (Faulkner et al., 2011; Johri et al., 2014). Strike-slip faults are one of the predominant fault types and are widely distributed across various geological settings, including plate boundaries, intraplate, or in sedimentary basins, where they substantially influence earthquakes and geological fluid dynamics (Sylvester, 1988; Mann, 2007). Strike-slip faults, particularly large-scale strike-slip fault zones or deformation zones, develop in segments and change dramatically in structural styles along the strike (Sylvester, 1988; Dooley and Schreurs, 2012). Several main fault slip surfaces and fault cores tend to develop in large-scale strike-slip fault zones or at stepovers (Faulkner et al., 2010; Lin et al., 2021). The damage zones associated with strike-slip faults can be divided into several types, including small-scale wall damage zones, large-scale damage zones, intersection damage zones, linking damage zones, and overlapping zones, all of which substantially influence fault and fracture connectivity (Yao et al., 2024). The fracture systems related to strike-slip faults predominantly comprise R, R', Y, and P shear fractures, with relatively less tension (T) fracture development (Dooley and Schreurs, 2012). Structural styles (e.g., as single fault segments, extensional overlaps, contractional overlaps, tails,

and bends) (Zeng et al., 2024b; Zhu et al., 2024), material properties, and structure evolution stages (Dooley and Schreurs, 2012) collectively influence fracture types and connectivity. As exploration targets are usually present in deeper unconventional petroleum reservoirs, geologists have discovered that intraplate strikeslip fault zones (especially within the basin) play essential roles in the migration and accumulation of petroleum in areas that display small tectonic deformation (Ma et al., 2022; Du et al., 2024). Structures in strike-slip-dominated regimes have been investigated through seismic interpretation, field investigations, numerical modeling, and physical modeling studies. However, considerable gaps remain in our understanding of the complex three-dimensional (3D) geometry of strike-slip fault zones and their associated fracture systems, particularly regarding their control on fluid flow patterns (Dooley and Schreurs, 2012).

The fractured reservoirs controlled by strike-slip fault zones located in the Shuntuoguole Low Uplift (SLU) are one of the most profound and deepest petroleum exploration fields in China, with an estimated reserve of $\sim 12.5 \times 10^9$ barrels of oil equivalent (Yang et al., 2021b; Wang et al., 2024). Similarly, the Sichuan Basin (He et al., 2023) and the Ordos Basin (Meng et al., 2023) in China have also developed a series of strike-slip fault zones within deep and ultradeep petroleum reservoirs (Jia et al., 2022). However, fracture data obtained from various sources exhibit considerable variability and discontinuity in scale. These include strike-slip fault zones (principal displacement zone (PDZ)) with multiple fault slip surfaces and are segmented along the strike from seismic data, faults or large-scale fractures with a single discontinuity plane in seismic data, small-scale fractures observed in cores and image logs, and microfractures identified in thin sections. The classical quantitative characterization parameters and correction methods for fractures from boreholes are often inadequate, particularly for high-angle fractures in vertical wells, in which the linear fracture density correction error tends to be substantial (Cao et al., 2024). Consequently, quantitatively evaluating faultcontrolled fractures across different scales remains a substantial challenge, especially when assessing the heterogeneity along the fault strike. This limitation complicates the selection of promising exploration targets.

To address these challenges, this study aims to quantitatively characterize fracture intensity and dip angle based on seismic data, cores, and image logs and through verification with published sandbox physical simulation results. Furthermore, this study analyzes the in-situ heterogeneous distribution characteristics of fracture intensity and dip angle within the structural framework of strike-slip fault systems. The findings on the in-situ distribution and development characteristics of fault-controlled fractures in this study can better guide the development of ultradeep fractured reservoirs.

2. Geological setting

2.1. Location

The Tarim Basin is a large petroleum-rich basin with a continental crust basement that displays a complex tectonic evolution history (Jia, 1999; Yang et al., 2020a). The Tarim Basin is divided into 16 secondary units based on the morphological characteristics of the crystalline basement. The SLU is located between the Manjiaer Depression in the east and the Awati Depression in the west (Fig. 1). The SLU connects the Tabei Uplift in the north and the Tazhong Uplift in the south. The oil field in the north SLU has reached industrial petroleum production capacity in fault zones

(Fig. 2), such as the Shuntuo No. 1 (SF1) and the Shuntuo No. 5 (SF5) strike-slip fault zones (Jiao, 2018).

2.2. Stratigraphy

The sedimentary strata preserved in the SLU are at a depth of ~10 km. The strata comprise a Sinian-Devonian marine sequence, a Carboniferous-Permian marine-terrestrial transitional sequence, and a Triassic-Quaternary terrestrial sequence (Fig. 3) (Jia and Wei, 2002). The limestone and dolomite strata in the Upper Cambrian and Middle-Lower Ordovician exhibit excellent reservoir properties in the SLU (Jiao, 2018; Ma et al., 2022). The tectonic evolution in the SLU is dominated by slow subsidence (Chai et al., 2020). The Ordovician strata have a gentle dip angle, with the current structural slope of the top of the Middle Ordovician at 0.13° towards the east direction and 0.1° to the south (Qi, 2020).

2.3. Structure

The structure in the SLU and its adjacent areas can be divided into several systems of "parallel strike-slip fault zones perpendicular to thrust faults" (Fig. 1) (Wang et al., 2020; Deng et al., 2021). Seismic data show that the vertical development depth of those strike-slip fault zones is >10 km, with a cumulative slip distance of 0.5-2 km (Huang, 2019). Multi-stage fault activity caused the connection and superimposition of the strike-slip faults into several large strike-slip fault zones. Based on the scale and developmental history, the large-scale strike-slip faults in the central and northern Tarim Basin can be classified as the main strike-slip fault zones (PDZ) and second-order faults (Jiao, 2017, 2018) or first- or second-order faults (Wang et al., 2022b). Largescale PDZs in the SLU are vertically or nearly vertically oriented and extend from the Precambrian basement to the top of the Middle Ordovician and en echelon normal fault zones in the overlying clastic strata. The deep, middle, and shallow parts of faults developed sequentially at different periods and formed in three stages during the Middle Caledonian, the Late Caledonian, and the Middle-Late Hercynian (Wang et al., 2020).

Stepover zones affect the main fault slip surfaces, leading to internal structure complexity and strong structural heterogeneity. Linking damage zones are developed as a result of secondary deformation between two fault segments through their interaction and linkage (Choi et al., 2016). The variance attribute slice from underground seismic data shows that the width of the linking damage zone is larger along fault traces (Fig. 4). Stepovers also typically occur at intersections of second-order and main faults, or at changes in fault strike.

2.4. Reservoir

The accumulation of oil and gas in the SLU is characterized by "local hydrocarbon sources, vertical transportation, late accumulation, and fault-controlled enrichment" (Jiao, 2017; Qi, 2020). The mudstone and limestone layers that overlie the Upper Ordovician Sangtamu Formation act as regional caprocks, and the shale of the Lower Cambrian Yueertus Formation is recognized as the source rock in SLU (Yun and Cao, 2014; Yang et al., 2021b).

Drilling, logging, and core data show that the fracture system controlled by the strike-slip fault zone is not only the seepage channel for oil and gas flow but also the main storage space in the ultradeep carbonate reservoir in the SLU (Wang et al., 2020; Kuang et al., 2021). Full diameter core analysis reveals that the average porosity is 2.1%, with 60% of the samples having a porosity less than 2% (Qi, 2020). Permeability is mainly distributed within 0.01–5.52 mD, and 72% of the tested samples exhibit a measured

permeability <1 mD (Qi, 2020). The aforementioned porosity and permeability data imply the relatively limited contribution of the pores in the matrix to the effective reservoir space. In contrast, it is found that the cavities, fractures, and dissolution holes along with fractures formed in brittle carbonate rocks by the multistage strike-slip faults and through fluid dissolution transformation are favorable storage spaces (Jiao, 2018).

3. Materials and methods

To study the characteristics of faults and fractures controlled by deep underground strike-slip fault zones, this study synthesized available data from various sources, including seismic data, cores, and image logs, and verified and compared them with sandbox simulation results published in the literature (Dooley and McClay, 1997; Dooley et al., 1999). These datasets were further classified based on their sources and types. Natural fractures in the SLU can then be divided into two observational scales: large-scale fractures in seismic data and small-scale fractures in cores and image logs. Subsequently, two-dimensional (2D) fracture intensity and porosity data were used to more accurately and quantitatively analyze the dip angle and development degree of fractures. Finally, the heterogeneity characteristics and influencing factors of fractured reservoirs controlled by strike-slip faults were analyzed. The area of 3D seismic data used in the study is ~3200 km², while the cumulative length of cores from 14 coring wells is 223 m. The cumulative length of image logs from 8 wells is 4393 m.

The observation in this study was compared with scaled sandbox models of Dooley et al. (1999). These models were performed in a 100 cm \times 60 cm rig filled with 10 cm of quartz sand layers as the rock analog. The analog experiment would scale to about 100 km \times 60 km \times 10 km in real-world dimensions. Releasing and restraining stepovers were produced with thin moving plates at the base of the sand. Dooley et al. (1999) provided

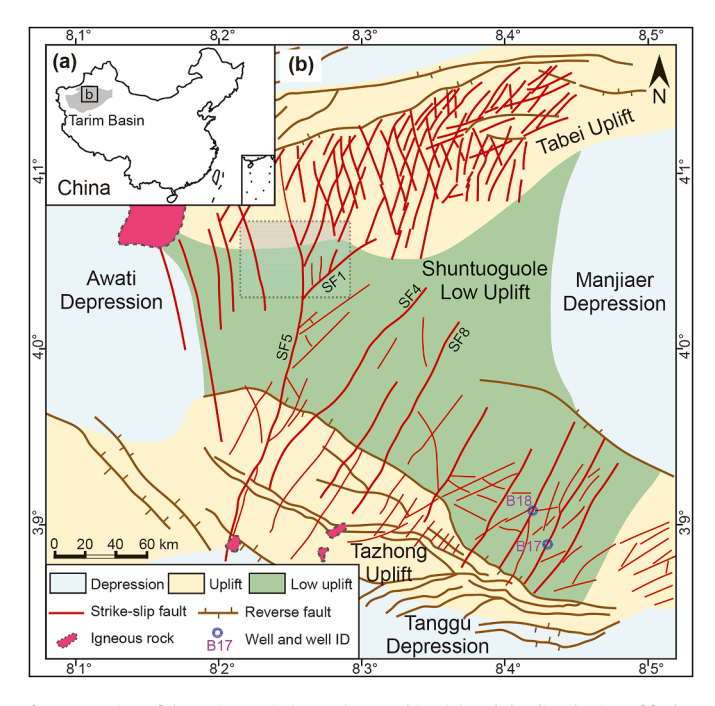


Fig. 1. Location of the Tarim Basin in northwest China (**a**) and the distribution of faults in the central and northern Tarim Basin (**b**). SF1, Shuntuo No. 1 strike-slip fault; SF5, Shuntuo No. 5 strike-slip fault; SF4, Shuntuo No. 4 strike-slip fault; SF8, Shuntuo No. 8 strike-slip fault. According to Huang (2019), Teng et al. (2020), Wang et al. (2020), Yun (2021).

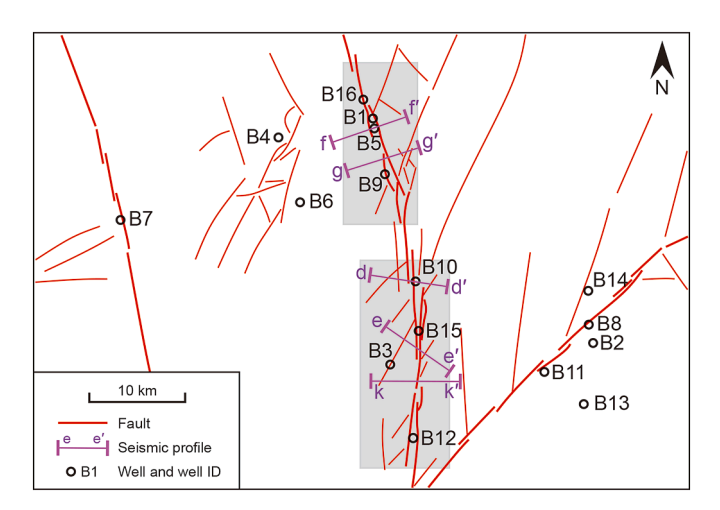


Fig. 2. Well locations and seismic profiles in the study area (the gray semitransparent area found in Fig. 1).

images of vertical sections through their models (Figs. 5 and 8 from their paper), which were used for this study.

Cores or image logs are usually the primary source of underground fracture data, which can provide valuable bedding and fracture data for subsurface rocks (Ortega et al., 2006). Based on the combination of the dimensions of measurement and sampling, the abundance of fractures (P_{xy} scheme, where x is the dimension of the observation and measurement region, and v is the dimension of the fracture parameters) is quantitatively determined using various parameters, such as density or frequency (P_{00} , P_{10} , P_{20} , and P_{30}), intensity (P_{10} , P_{21} , and P_{32}), and porosity (P_{00} , P_{11} , P_{22} , and P_{33}) (Dershowitz and Herda, 1992). One-dimensional linear fracture density (P_{10}) refers to the number of fractures per unit length of the scanline in the normal direction to the same set of fractures. Ideally, the linear fracture density should be measured perpendicular to the normal vector of fractures in a set that is nearly parallel. However, it is difficult to measure high-angle fractures in the normal direction of the fracture surface in the vertical wells underground. In addition, there are sampling biases related to the measurement and calculation of the scanline method, for example, orientation bias, size bias, truncation bias, and censoring bias (Zeeb et al., 2013, and reference therein). To address this problem, a correction method with a consideration of the fracture apparent density deviation was proposed (Terzaghi, 1965). The Terzaghi correction method of P_{10} is equivalent to correcting the scanline to the normal direction for fractures in a set. The Terzaghi correction method of P_{21} (2D fracture intensity) overcomes the instability of fracture density caused by the change in sampling window (Bisdom et al., 2014). However, P_{10} logged from core or borehole image logs may be unreliable when the joints are clustered and vary across magnitudes (Peacock, 2006). Therefore, P_{21} and P_{22} (2D fracture porosity) corrected by the Terzaghi method (Sanderson and Nixon, 2015) are chosen to characterize the degree of fracture development in this study.

Although the fracture density varies with the fracture scale, fractures within a specific range of scales can provide representative fracture samples (Ortega et al., 2006). Therefore, fractures in different finite-scale ranges from the core or seismic data are also representative. In this study, faults and large-scale fractures refer to the single discontinuity surfaces in seismic data (it is not easy to distinguish them due to the small vertical fault displacement). In this study, typical seismic profiles and corresponding fault interpretations presented in the references (seismic profiles and main fault interpretations remain consistent with Fig. 5 of Lin et al.

(2021) and Fig. 5 of Sun et al. (2021)) were selected to reduce the subjective errors caused by seismic profile selection and detailed structural interpretation. The detailed structure interpretations are based on the recognition results of U-net artificial intelligence method (Wu et al., 2022). Small-scale fractures refer to the fractures observed by the naked eye in the core (Lyu et al., 2021), identified by image logs and predicted using the comprehensive fracture index (CFI) method from well logging data (Lyu et al., 2017). Their dip angles and extension length were obtained through direct measurements using rulers, protractors, and carpenters' protractors (Liu et al., 2020b; Lorenz and Cooper, 2020). The fractures based on the data interpreted by image logs were also considered small-scale.

The FracPaQ toolbox was used to obtain the fracture dip angle and length (Healy et al., 2017) in the sandbox models of Dooley et al. (1999) and in seismic interpretations of the PDZ. The software divides a nonstraight fracture into several straight lines when calculating the dip and length. Rather than histograms, the cumulative distribution method can be applied to effectively avoid binning problems (Zeeb et al., 2013). Considering that the fracture length affects the estimate of the cumulative probability of fracture dip, the error caused by the fracture length was corrected using fracture length as the weight when calculating the cumulative probability of fracture inclination.

4. Results

4.1. Fracture types

A reasonable classification of fractures based on their origin mechanics is critically important to quantitatively characterize their behaviors in reservoirs (Lorenz and Cooper, 2020). Without a clear definition and classification of fractures, the accuracy of prediction, analysis, and model buildup would be highly restricted (Wennberg et al., 2016; van Der Voet et al., 2020; Zeng et al., 2022). Table 1 summarizes various fracture classifications defined in the past. In this study, the classification proposed by Zeng and Li (2010) and Zeng et al. (2016) was used because of the different evolution processes and control factors of fractures, namely, tectonic fractures, abnormal high-pressure-related fractures, and stylolites.

4.1.1. Tectonic fractures

Tectonic fractures are the dominant type of fracture and typically consist of two straight fracture surfaces with no, or only a small opening between/or often found in an en echelon arrangement (Zeng et al., 2016; He et al., 2019). Such fractures are commonly observed in drill cores or in image logs, where they display as sinusoidal arcs, depending on their dip (Figs. 5, 6(a), 6 (b)). Most tectonic fractures (87%) are completely or partially filled with calcite and a small amount of grayish-black siliceous or grayish-green argillaceous material and can thereby also be termed "veins" (Fig. 6(c)) (Bons et al., 2012). Traces of residual oil can be observed in some partially filled fractures (Fig. 6(e)). The appearance, filling, and aperture of fractures within the same set of fractures are relatively similar. The vertical distribution of fractures is clearly affected by the layer interfaces and stylolites. Here, termination or bifurcation of fractures, as well as changes in fracture density can be observed.

4.1.2. Abnormal high-pressure-related fractures

Abnormal high-pressure-related fractures, also known as "expulsion fractures" (Lorenz and Cooper, 2020), or "natural hydrofractures" (Bons et al., 2022), are formed by the abnormally high fluid pressure during the thermal evolution of organic matter

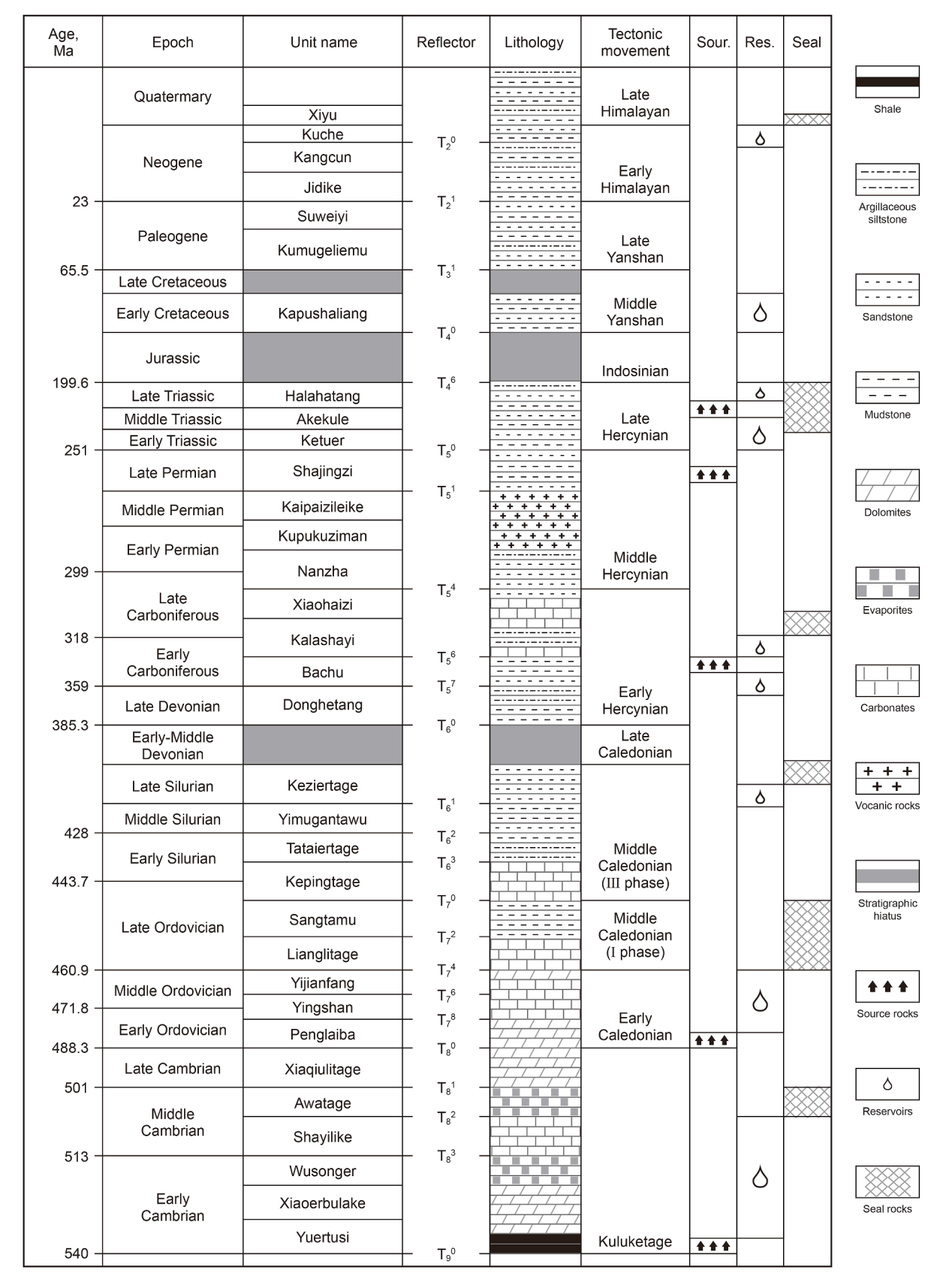


Fig. 3. Schematic stratigraphy and hydrocarbon source rocks, reservoirs, and cap rocks in the SLU, Tarim Basin (according to Wang et al., 2020).

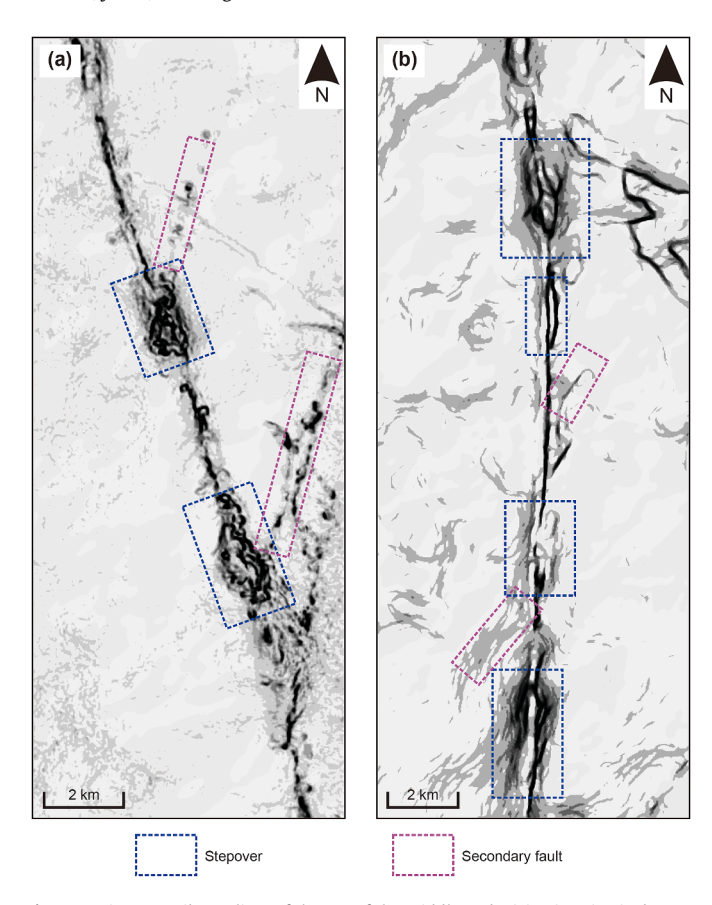


Fig. 4. Variance attribute slices of the top of the Middle Ordovician in seismic data. In the stepover, the PDZ becomes wider and displays more fault traces. Secondary faults can be recognized near the stepovers. Fig. 4(**a**) and (**b**) illustrate the gray area located in the north and south parts of Fig. 2, respectively.

(Zeng and Li, 2010) or fractures propagating when buoyant fluids reach critical vertical length (Bons et al., 2022). Abnormal high-pressure-related fractures usually have short extensions, variable occurrences, large roughness and aperture (Zeng et al., 2016). The abnormal high-pressure-related fractures in the SLU are fully or partially filled with calcite with a certain amount of irregular rock breccia (Fig. 6(f)). The fracture surface shows a relatively high roughness and usually branches at the end. However, the probability of cores encountering typical abnormal high-pressure-related fractures is not high and is only encountered in Wells B14 and B17.

4.1.3. Stylolites

A large number of stylolites are also well developed in carbonate strata (Fig. 7). Two types of stylolite, that is, bedding-parallel sedimentary stylolites and tectonic stylolites with large angles between beddings, can be observed in the study area. Botrh are mainly of the "seismogram-pinning" or "suture-and-sharp-peak" types in the classification of Koehn et al. (2016). The stylolites tend to consist of a continuous clay-rich layer, which would constitute a baffle for fluid flow, but may also show calcite precipitation on the sides of stylolite teeth, which indicates fluid leaking across the stylolitess (Koehn et al., 2016; Gomez-Rivas et al., 2022). Here the stylolites are therefore considered a fluid flow channel rather than a barrier (Heap et al., 2018). However, only a few tectonic stylolites are encountered in Wells B8 and B17 only, and the sedimentary stylolites are not frequent in the main

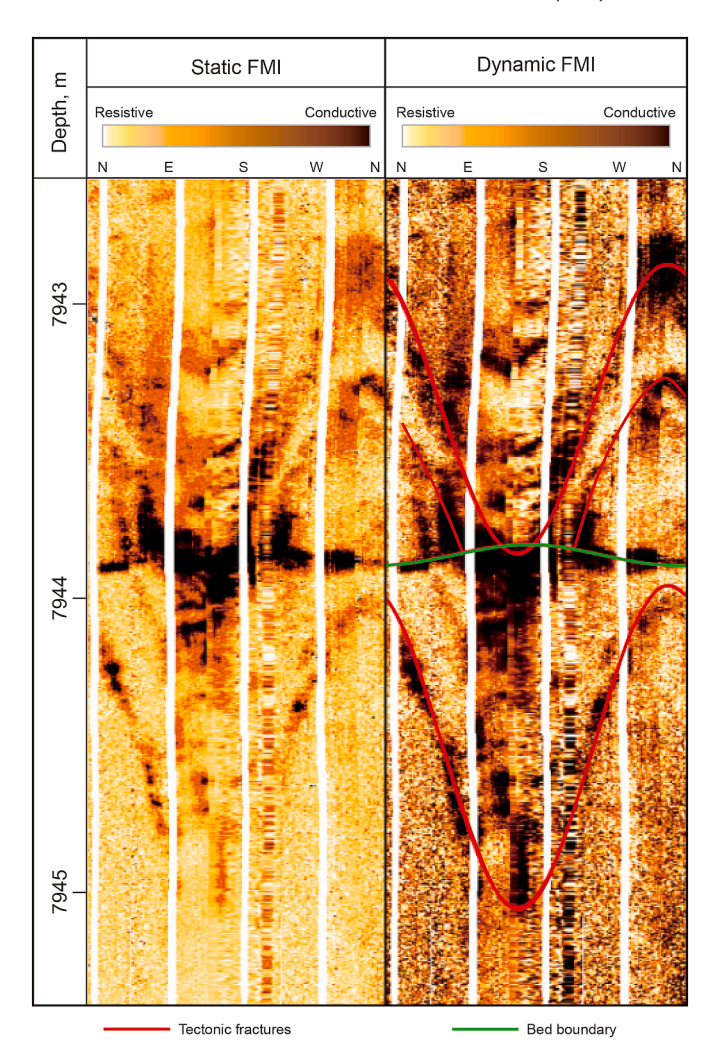


Fig. 5. Tectonic fractures in image logs (7942.6–7945.4 m in the Yingshan Formation from Well B3). The bed boundary (green line) limits the vertical extent of high-angle tectonic fractures (red traces).

production section. Therefore, we do not consider stylolites as a primary controlling factor on reservoir quality.

4.2. Characteristics of faults and tectonic fractures

Among the structures described in the previous section, tectonic fractures are the most abundant compared with abnormal high-pressure-related fractures and stylolites. Thus, it is assumed that faults and tectonic fractures control the storativity and permeability of the ultradeep reservoir in the SLU. It is, therefore, critical to gain insight in the distribution characteristics and, in particular, the heterogeneity in density and orientation of these faults and tectonic fractures.

4.2.1. Faults in seismic profiles

Seismic profiles perpendicular to the strike of the PDZ fault zone show positive or negative flower structures in stepovers and a single main fault in the non-stepover. Five typical profiles (Fig. 8, the position is shown in Fig. 2) were selected to quantitatively analyze dips of faults, and the main faults of these profiles have been interpreted in the references (Lin et al., 2021; Sun et al., 2021). The seismic profiles were compared with the same fault interpretation in the time and depth domains. The horizontal and

vertical scales of the depth domain profiles are equal, as shown in Fig. 8. Interpreters tend to use seismic profiles with a vertical scale 5-20 times the horizontal scale in the time domain to show the strike-slip fault zone in the SLU (Fig. 8) (Lin et al., 2021; Sun et al., 2021). The relatively smaller horizontal scale makes the visual dip angle of faults and fractures steeper. To analyze the dip angles of faults, we calculated the cumulative probability curves of the interpreted fault dips at the same horizontal and vertical scales (Fig. 9(a)). All angles above 75° are classified as "high-angle dips" and those below 75° are "medium-to-low-dip". The proportion of high-angle parts in the negative flower stepover (60% in gg') is higher than that in the positive flower stepover (43% in ff') in the north SF5. In the middle N-S strike fault zone, the proportion of high-angle parts in the non-stepover segment (58% in kk') is higher than that of negative flower stepover (36% in ee'), while the proportion in the positive flower stepover (23% in dd') is the lowest. The proportions of high-angle faults and fractures in the northern strike (NNW-SSE) are lower than that in the N-S strike of the middle SF5.

4.2.2. Fractures in boreholes

Fracture density and dip parameters derived from core measurements and image logs can be utilized to establish the cumulative probability curve of fracture dip (Fig. 9(b) and (c)). It was observed that the corrected cumulative frequency curve of all recorded fractures exhibited a linear increase of up to about 75° followed by a distinctly steeper increase in the high-angle domain (Fig. 9(b)). High-angle fractures constitute about 60% of the total sample. Again, this percentage is slightly smaller (especially for data from image logs) when the data are length-weighted. The higher percentage of high-angle fractures in cores and image logs compared to that in the seismic images is (at least in part) due to the fact that the true dip angle can be measured.

The cumulative frequency curves vary considerably between individual drill cores (Fig. 9(c)). Wells B1, B4, and B15 show no or very few high-angle fractures. In contrast, Wells B2 and B3 display <10% high-angle fractures. The remaining Wells B6 and B7 show approximately equal proportions of high-angle and medium-to-low-dip fractures. Thus, fracture-angle distributions vary greatly laterally, showing the high heterogeneity in these stepover structures.

The researchers further calculated P_{21} and P_{22} of the small-scale tectonic fractures from the core observation and image logs. The average fracture aperture of a well is defined as P_{22} divided by P_{21} . The results are plotted as a function of distance from the main fault (Fig. 10). It displays a general power-law decrease of all fracture intensity parameters and porosity with increasing distance from the fault, with P_{22} showing the strongest decrease.

5. Discussion

5.1. Control of secondary faults and fracture occurrence by strikeslip faults

The results of sandbox experiments from previous studies (Dooley and Schreurs, 2012 and reference therein) on strike-slip faults and associated structures have substantially enhanced the understanding of the internal architecture of strike-slip fault systems. These related structures include Riedel shears (Tchalenko, 1970), pull-apart basins (Dooley and McClay, 1997), and strikeslip "pop-up" structures (Schellart and Nieuwland, 2003), corresponding to three typical structural types of strike-slip fault systems, that is, pure strike-slip, transtensional stepover, and transpressional stepover, respectively. Sandbox experiments focusing on pull-apart basins (Dooley and McClay, 1997) and segmented strike-slip fault systems (Dooley et al., 1999) provide a robust dataset for the quantitative analysis of typical strike-slip fault structural styles. These experimental results (Fig. 11) offer a valuable basis for comparison with the observational data of this study from the SLU.

The experimental results clearly demonstrate that the width of damage zones is considerably larger at linking stepover zones compared with that at other sections along the fault (Fig. 11). Faults and fractures away from the stepover structures predominantly exhibit steep apparent dip angles ($>60^\circ$) with $\ge 50\%$ of them exceeding 75° (Fig. 12). The distribution of dip angles undergoes considerable changes in both transpressive and transtensional stepovers. In transpressional pop-up structures (Fig. 12(a)), all apparent dip angles are approximately equally distributed, with only 20%–30% of faults and fractures exhibiting high angles. In contrast, faults and fractures in transtensional stepovers are generally steeper, with 25%–50% of them displaying high angles (Fig. 12(b)).

This pattern is consistent with the borehole data in the SLU (Fig. 9(b) and (c)), where the proportion of medium-to low-angle parts increases substantially at the stepover zones (Wells B1 and B15). High-angle fractures are also rarely developed in areas adjacent to the stepover of second-order faults (Well B4). In contrast, away from a stepover along strike-slip faults (e.g., Well B7) and second-order fault zones (Well B3), high-angle fractures dominate, with medium-to-low-dip fractures accounting for a relatively small fraction. Similarly, high-angle fractures are predominant in fault damage zones (Wells B2 and B6) that are far away from the PDZ. Overall, the proportion of medium-to-low-dip angle fractures in the stepover can reach up to about 90% but is less than 50% in other areas.

Table 1 Classifications and basis of fracture types.

Classification basis	Types	References
Genetic classification	Natural fractures (related to natural deformation of the rock), induced fractures (induced artificially, e.g., by drilling, handling, coring, drilling, fluid injection, etc.)	Zeng et al., 2015; Lorenz and Cooper, 2017
Naturally occurring classification	Tectonic fractures, regional fractures, contractional fractures, surface-related fractures	Nelson, 2001; Nelson, 2019
Geological genetic classification	Tectonic fractures, diagenetic fractures, overpressure-related (abnormal high-pressure-related) fractures	Zeng and Li, 2010; Zeng et al., 2016
Characterize from image logs	Conductive fractures, resistive fractures, induced fractures, faults, bedding	Rashid et al., 2020
Identified from image logs using resistivity	Open fractures, closed or mineralized/filled fracture, partially open fracture, fault, induced fracture	Hennings et al., 2012
Fracture dip angle Fracture scale	High-angle, intermediate-angle, low-angle, bed-parallel fractures Large-scale natural fractures, medium-scale natural fractures, small-scale natural fractures, microscale natural fractures	Lorenz and Cooper, 2020 Lorenz et al., 2006; Lyu et al., 2021

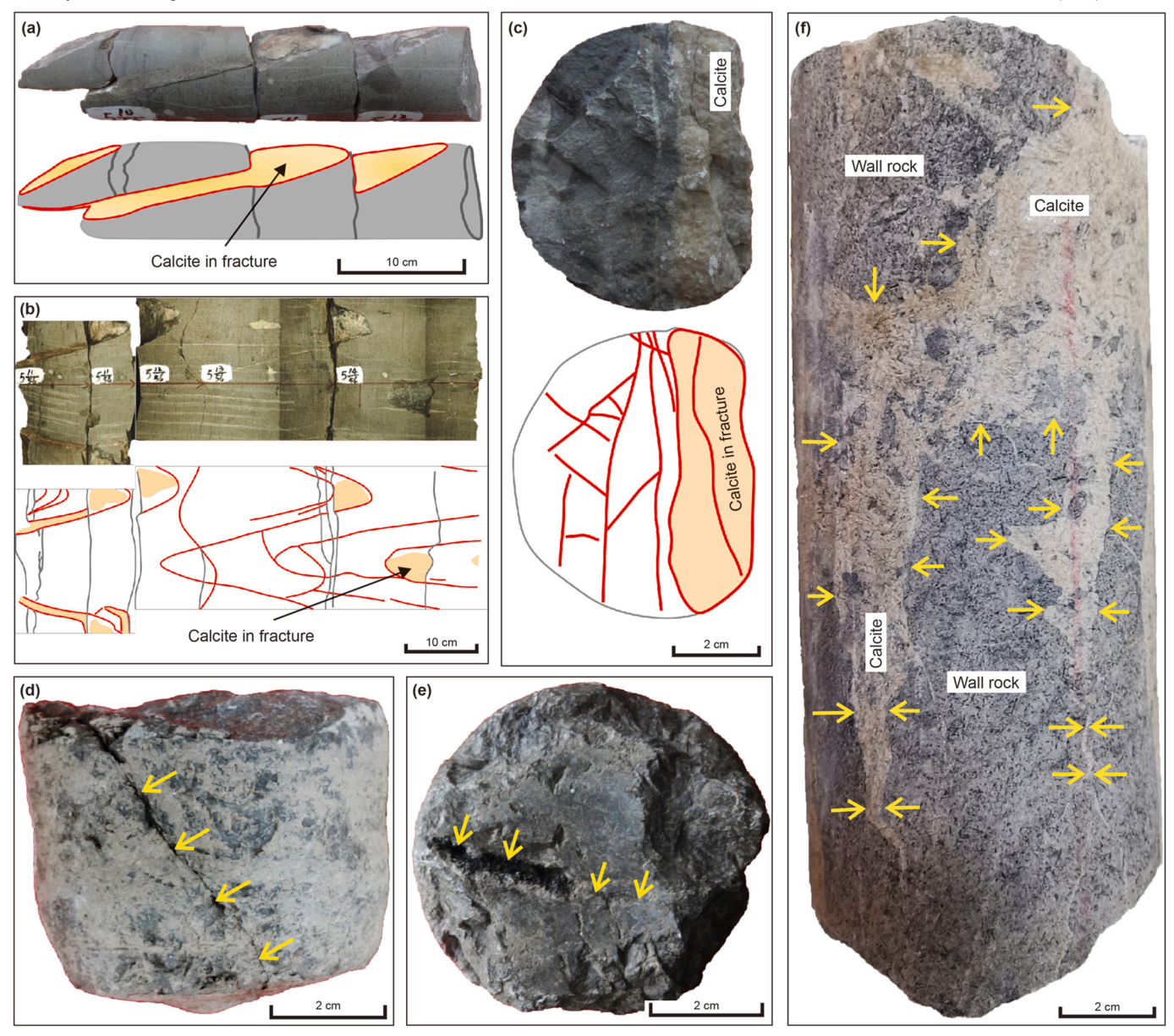


Fig. 6. Examples of fractures in cores (the red lines are fractures, and the light-orange area is calcite vein in the sketch figure). (a) En echelon calcite veins, 7326.47–7326.84 m in Well B17. (b) En echelon tectonic fractures in a roll sweep figure, 7326.52–7327.08 m in Well B17. (c) Tectonic fractures in the cross-section of the core, 7327.56 m in Well B17. (d) Medium-to-low-dip tectonic fracture, 7468.50-7468.56 m in Well B9. (e) Partially filled medium-to-low-dip tectonic fracture with traces of oil on the surface of crystals, 7481.3 m in Well B9. (f) High-fluid-pressure hydrofracture filled with calcite and wall rock breccia clasts, 6468–6468.21 m in Well B18.

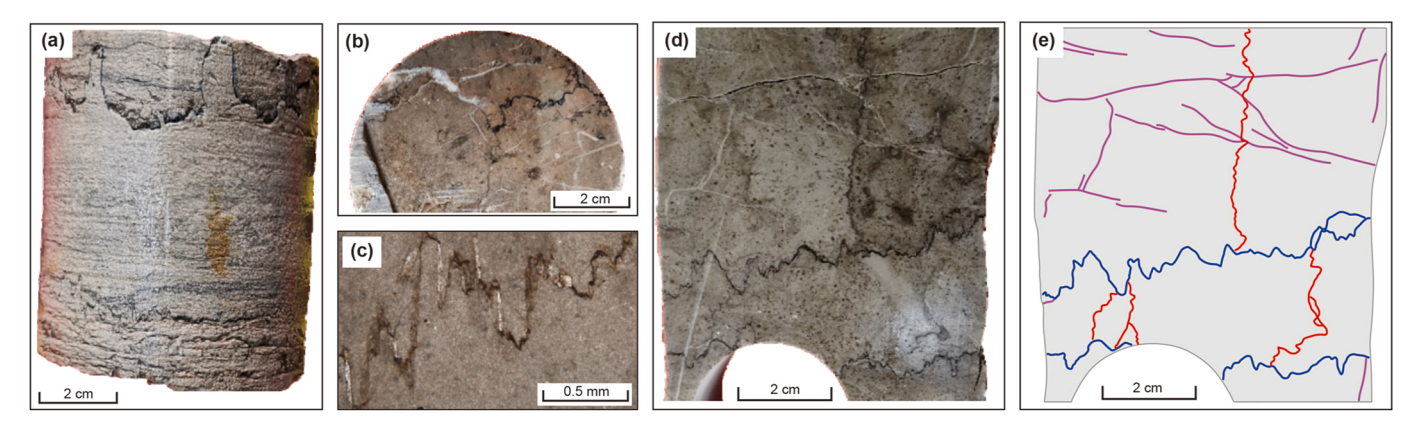


Fig. 7. Stylolites in core and thin sections. (a) Sedimentary stylolites, 7504.73–7504.83 m in Well B13. (b) Stylolites viewed from above in a cross section of a core in Well B4, 7509.68 m. (c) Stylolite with calcite cement, 7676.50 m in Well B1, polarized light. (d) Sedimentary and tectonic stylolites in a core, 7352.52–7352.68 m in Well B8. (e) Sketch figure of (d) with high-angle tectonic stylolites, bedding-parallel stylolites, and drilling-induced fractures drawn in red, blue, and magenta, respectively.

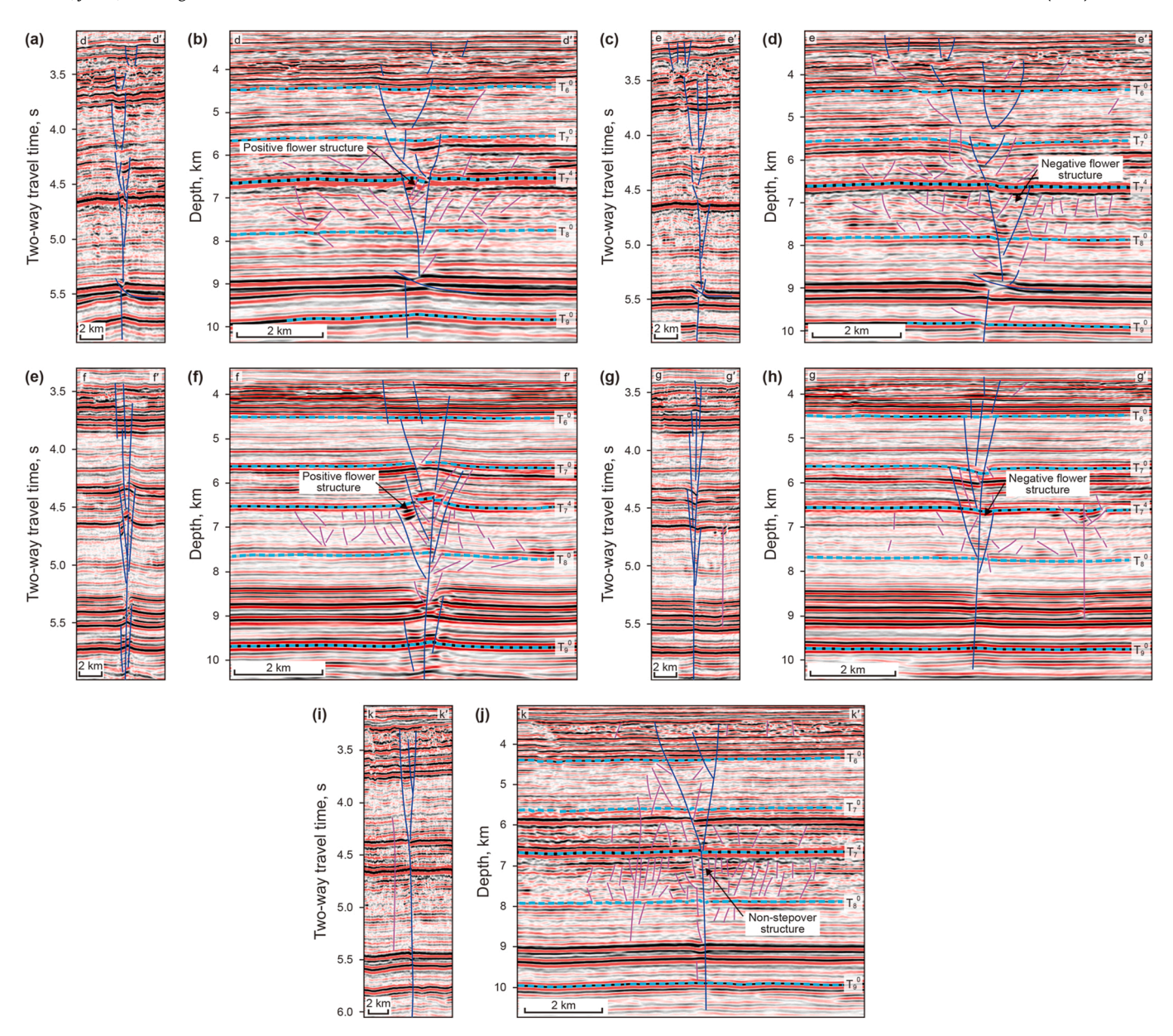


Fig. 8. Strike-slip fault zones and their associated secondary faults and large-scale fractures in seismic sections. The solid dark blue lines represent the main faults interpreted in the reference literature. The solid magenta lines represent the detailed interpretations of secondary faults and large-scale fractures. The light blue dashed lines represent the strata interfaces. The vertical scales of (a), (c), (e), (g), and (i) are in the time domain, while those of (b), (d), (f), (h), and (j) are in the depth domain. (a) The positive flower structure in the middle of the SF5 is located at dd' in Fig. 2. The interpretation of the main fault refers to the section BB' in Fig. 5 of Lin et al. (2021). (b) Seismic section of (a) in the depth domain and structure interpretation. (c) The negative flower structure in the middle of the SF5 is located at ee' in Fig. 2. The interpretation of the SF5 is located firing Fig. 2. (f) Seismic section of (e) in the depth domain and structure interpretation. (g) The negative flower structure in the north of the SF5 is located at gg' in Fig. 2. (h) Seismic section of (g) in the depth domain and structural interpretation. (i) The non-stepover structure in the middle of the SF5 is located at kk' in Fig. 2. (j) Seismic section of (i) in the depth domain and structural interpretation. (e), (g) and (i) refers to sections a', b', and c' in Fig. 5 of Sun et al. (2021), respectively.

The cumulative probability curve of the dip angle, which is weighted by fracture length, exhibits notable differences compared with the unweighted curve (Fig. 9(b)). The statistical analysis of fracture dip angles must incorporate the distribution of fracture lengths to minimize biases introduced by variations in fracture scale. A cumulative probability curve of dip angle weighted by fracture length can be employed to effectively avoid potential binning issues, thereby providing a more accurate and representative characterization of fracture properties.

Previous studies generally suggest that faults and fractures controlled by strike-slip faults are steep, with medium-to-low-dip

en echelon normal faults typically confined to overlying clastic strata (Wu et al., 2021). Consequently, faults interpreted from seismic profiles in the Lower to Middle-Ordovician carbonate sequences are usually characterized by high-angle dips. However, despite potential biases in the statistical analysis of apparent dip angles from seismic data and sandbox models, medium-to-low-dip true dip fractures constitute a substantial proportion of fractures observed in cores and image logs (Fig. 9(b) and (c)). This indicates that a considerable number of medium-to low-angle faults and fractures can develop within strike-slip fault systems, particularly in stepover segments. The alteration of the stress field

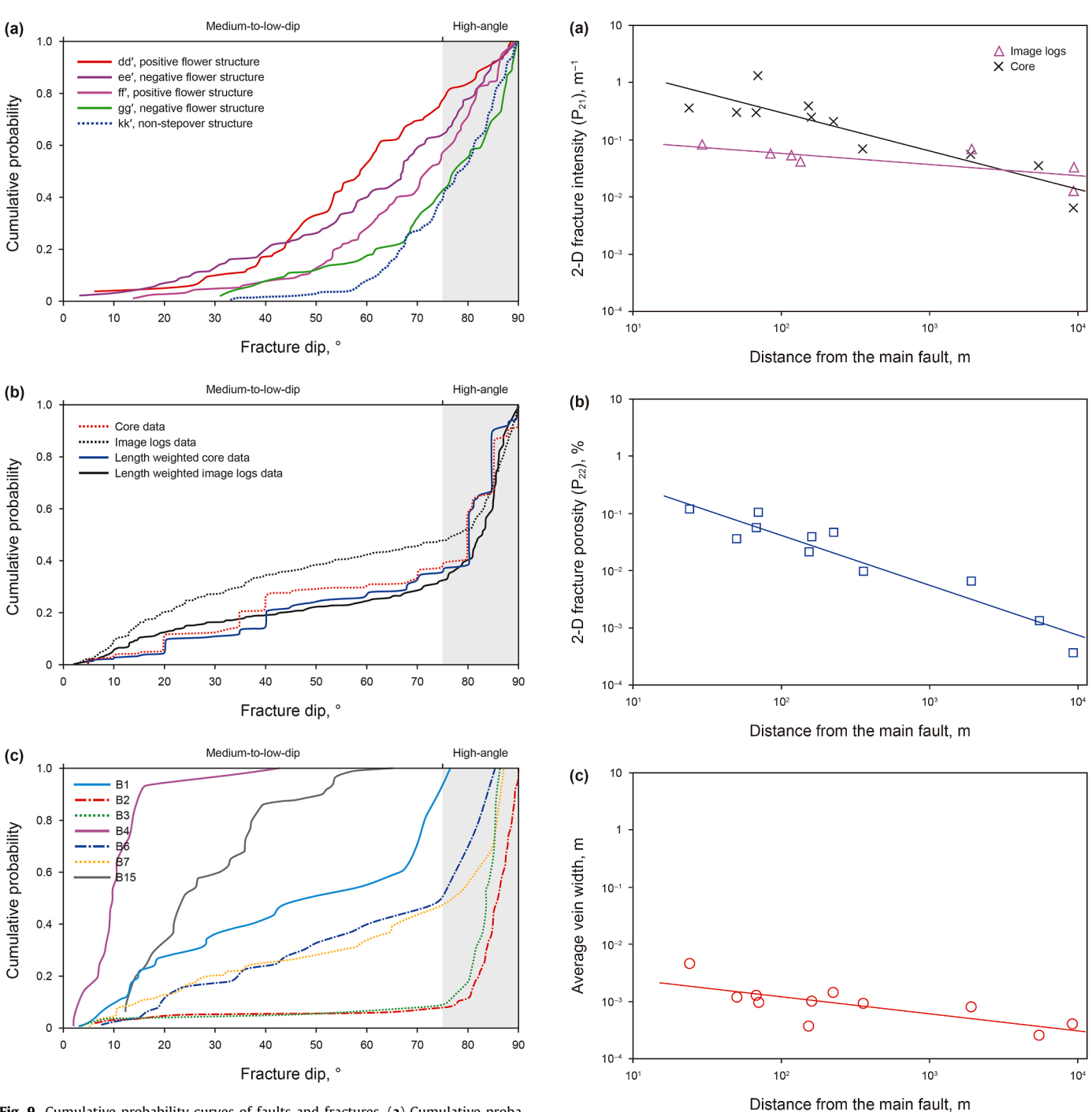


Fig. 9. Cumulative probability curves of faults and fractures. (a) Cumulative probability curves of all recorded apparent dip angles of faults and large-scale fractures based on seismic sections. Sections dd' and ff are positive flower structures and are also termed palm tree structures. Sections ee' and gg' are negative flower structures and are also called tulip structures. Section kk' is a non-stepover structure, displaying a single main fault in the Middle and Lower Ordovician to Cambrian. The proportion of high-angle faults and large-scale fractures in non-stepover structures (57% in kk') is considerably higher than that in stepover structures (19%, 33%, 43%, and 52% in dd', ee', ff', and gg', respectively). (b) Cumulative probability distribution of fracture dip angles that are observed in image logs (297 fractures) and drill cores (180 fractures). (c) Cumulative probability plot of dip angles of tectonic fractures inferred from image logs in different wells (fracture sample number: B1, 26; B2, 138; B3, 17; B4, 20; B6, 22; B7, 41; B15, 33).

at strike-slip fault stepovers (Nabavi et al., 2017) is likely the primary factor that drives the transformation of secondary fault properties into normal or reverse faults (Teng et al., 2020) and the

Fig. 10. Fracture intensity (\mathbf{a}), fracture porosity (\mathbf{b}), and vein width (\mathbf{c}) plotted against the distance from the main fault. Straight regression lines in the log-log axes indicate power-law relationships.

increased occurrence of medium-to-low-dip fractures from seismic to core scales.

5.2. Control of secondary faults and fracture abundance by strikeslip faults

The damage zone of a major fault is characterized by a considerably higher fracture density compared with the surrounding wall rock, with fracture densities decreasing progressively as the distance from the fault core increases (Brock and Engelder, 1977; Faulkner et al., 2011; He et al., 2019; Ma et al.,

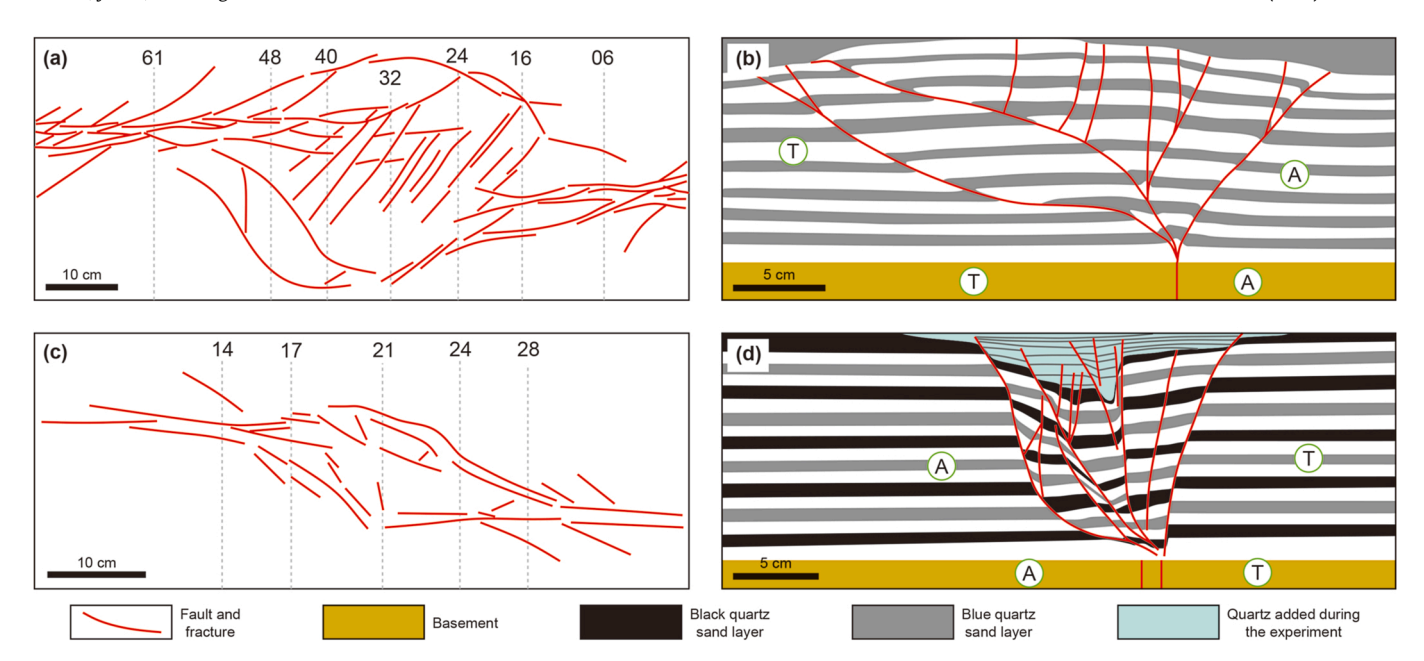


Fig. 11. Structural styles, fault and fracture characteristics of stepovers in the scaled sandbox models of Dooley et al. (1999). (a) Strike-slip "pop-up" structure. (b) Section 40 of Fig. 11(a) in this literature. (c) Strike-slip pull-apart structure. (d) Section 17 of Fig. 11(c) in this literature. Strike-slip movement is perpendicular to the image with T and A indicating movements toward and away from the viewer, respectively. The black, gray, and white stripes in Fig. 11(b) and (d) represent different colored quartz sand marker layers. The gray dotted line and corresponding numbers refer to the position and number of the vertical slices that were subjected to dip-angle and density analyses (Figs. 12 and 13). These figures are redrawn after Dooley et al. (1999).

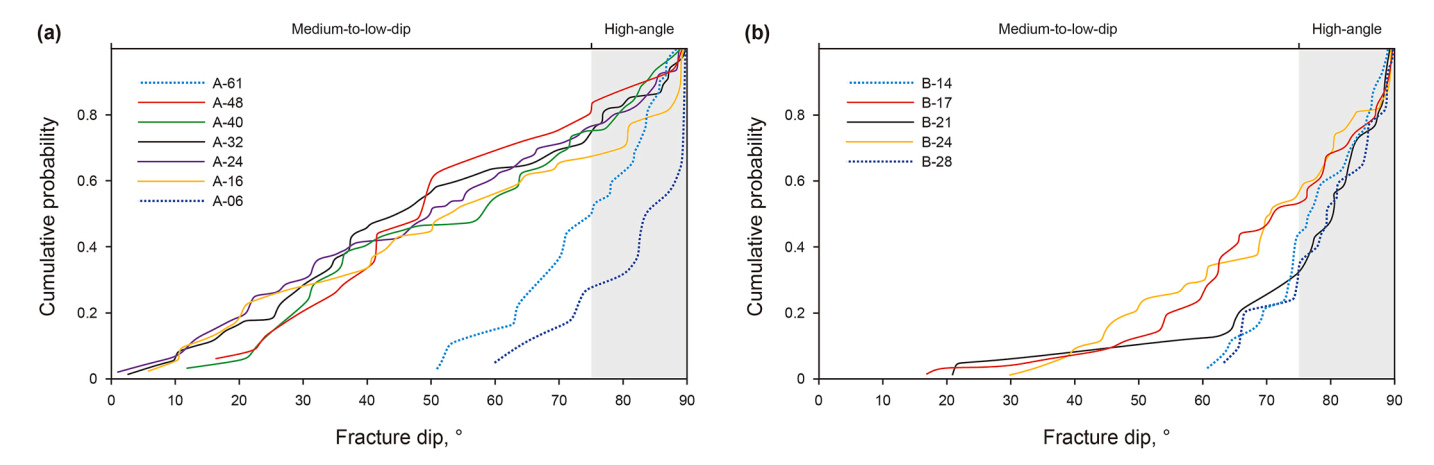


Fig. 12. Cumulative probability distributions of apparent fracture dip angles in the scaled sandbox models. (a) Fractures in a transpressional pop-up stepover (see Fig. 11(a) for the locations of the sections). (b) Fractures in a transtensional pull-apart stepover (see Fig. 11(c) for the locations of the sections). Sections at either extreme ends of the stepovers (A-06 and A-61 in (a) and B-14 and B-28 in (b)) are shown as dotted lines. These show a distinctly higher fraction of steep fractures compared with the other sections.

Table 2Variation trends of fracture development parameters with the distance from strike-slip faults.

Parameters	Formulas	Coefficient of determination
P_{21} in cores, m ⁻¹	$F = 6.69 \cdot r^{-0.673}$	0.81
P ₂₂ in cores, %	$F = 2.51 \cdot r^{-0.883}$	0.91
Average fracture aperture in cores, m	$F = 0.0049 \cdot r^{-0.299}$	0.56
P_{21} in image logs, m ⁻¹	$F = 0.143 \cdot r^{-0.195}$	0.55

2019). This spatial variation in fracture density as a function of distance (*r*) from the fault core can be described using a power-law relationship (Savage and Brodsky, 2011; Johri et al., 2014):

$$F = F_0 \cdot r^{-n} \tag{1}$$

Here, F represents the fracture density in units of number per meter, F_0 refers to constant equal to the fracture density at unit distance from the fault core, r is the distance from the fault core, and n denotes an exponent describing the decay rate of fracture density with distance.

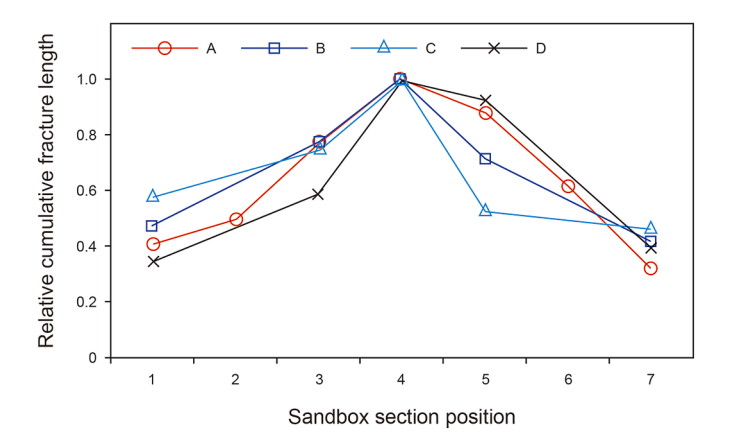


Fig. 13. Relative cumulative length of fractures at different positions of the stepover structure. Data A and B are adapted from Fig. 11 in this literature, while data C and D are adapted from Fig. 9 in Dooley and McClay (1997).

To date, there have been few published studies on the controlling effect of strike-slip faults on the development of small-scale fractures in (ultra) deep formations (He et al., 2019; Cao et al., 2023). This study demonstrates that the in-situ P_{21} , P_{22} , and fracture aperture all follow a power-law decay with increasing distance from the PDZ (Fig. 10). This indicates that fracture storage space is greatest at and near the fault. Among these parameters, P_{22} exhibits the steepest decay and the highest determination coefficient (Fig. 10 and Table 2), suggesting that fractured reservoir space decreases more rapidly than fracture intensity. Compared to core data, image logs primarily identify unfilled and semifilled fractures with low resistivity. The slower decrease in P_{21} observed in image logs implies that fractures closer to the main fault are more extensively cemented than those more distant from the fault.

Additionally, sandbox experiment results reveal that the cumulative fracture length in the central stepover can be up to twice that at the ends of the stepover (Fig. 13). Therefore, fracture densities along the main fault strike in stepover zones also exhibit considerable heterogeneity.

The CFI method, based on conventional well logging data, is used to predict the abundance of fractures near well trajectories (Lyu et al., 2017). A higher CFI value indicates greater fracture intensity. Using the CFI method, the researchers predicted the fracture abundances in inclined wells passing through fault zones (Fig. 14). These wells are located in a non-stepover (Fig. 14(a)), a transpressional stepover (Fig. 14(b)), and a transtensional stepover (Fig. 14(c)). The horizontal projection width of the predicted fracture zones is typically less than 100 m, with dense, unfractured wall rock separating these zones. In contrast, the width of damage zones identified by seismic attributes often ranges from several hundred meters to 3000 m (Ma et al., 2019; Zhao et al., 2021; Yao et al., 2023). When fracture zones are in close proximity, such as in the case of Well B5 located in a transpressional stepover, it becomes challenging to classify these zones as part of the same fault damage zone. In non-stepover and transtensional stepover segments, the width of the fault damage zone identified by seismic data often includes intact, unfractured rock sections with no developed fractures. Additionally, seismic data may fail to detect some fracture zones located at a considerable distance from the main fault surface. Due to the limitations of seismic resolution, seismic data can only provide a rough estimate of the extent of fault damage zones in complex fault systems. In contrast, the quantitative characterization of small-scale fractures offers a more accurate representation of the internal structure of fault zones.

5.3. Fluid activity and favorable targets of fractured reservoirs controlled by strike-slip faults

The in-situ P_{21} , P_{22} , and fracture aperture decrease with the increasing perpendicular distance from the PDZ (Fig. 10). Due to the superposition of fault damage zones controlled by multiple fault surfaces, stepover zones exhibit a greater volume of fractured rocks and a higher density of fault and fractures. The wider fracture zone and higher fracture intensity in the stepover are favor the migration and accumulation of hydrocarbons from the lower source rock to the reservoir (Cunningham and Mann, 2007; Ma et al., 2020). However, the strike and dip angles of individual faults and fractures substantially influence their contribution to reservoir productivity (Hennings et al., 2012). Consequently, the heterogeneity of fault-related fractures plays a critical role in the production of hydrocarbons and the selection of favorable exploration targets. The fluid production per unit pressure drop in development wells located in stepovers and non-stepovers (Liu, 2020) further demonstrates that fault stepovers are more favorable for the production of hydrocarbons (Fig. 15(a) and (b)). There is a considerable difference in fluid production per unit pressure drop between wells located in stepovers and non-stepovers within the SLU. Additionally, the fracture density in the central part of a stepover is considerably higher, creating conditions that are conducive to the accumulation and enrichment of hydrocarbons.

During drilling tests, nine high-yield wells with initial daily oil and gas equivalent production exceeding 1,000 tons were identified. These wells are primarily located along the PDZ extending in the NE-NW direction, such as SF4 and SF8 (Yang et al., 2020b; Wang et al., 2022a). The fault segment strike that hosts these high-yield wells aligns closely with the regional maximum principal stress direction (NE42.5 $^{\circ}\pm10^{\circ}$) (Yang, 2021). The researchers in this study analyzed the relationship between the initial daily production and the angle between the fault segment strike and the maximum horizontal principal stress (Fig. 15(c)). Results show that the daily oil and gas equivalent production decreases as the angle increases, indicating that the present-day in-situ stress considerably controls reservoir properties within the strike-slip fault zone. Specifically, the smaller the angle between the strike-slip fault segment and the maximum horizontal principal stress, the higher the production capacity. Previous research indicates that fractures with smaller angles relative to the strike-slip fault strike are more extensively developed in the SLU area (Yao et al., 2023). This implies that the angle between these fractures and the maximum horizontal principal stress is also smaller, resulting in larger fracture apertures compared with fractures with other orientations. Consequently, these fractures contribute more to porosity and permeability, enhancing hydrocarbon flow. Therefore, the strikeslip fault system not only controls fracture orientation but also plays a critical role in influencing oil production.

Mechanical stratigraphy is a critical factor that controls the development of faults and fracture systems, which in turn influences oil and gas accumulation and reservoir productivity (Zeng et al., 2023b). Mechanical stratigraphy divides stratified rocks into discrete mechanical units based on physical properties such as porosity, permeability, elastic properties, and brittle strength, the latter of which is typically defined by tensile strength, cohesion, and friction coefficient (Laubach et al., 2009). The characteristics of mechanical stratigraphy are determined by the types, properties, and limiting capacities of mechanical stratigraphic interfaces, which govern the vertical propagation of faults and fractures at various scales (Cao et al., 2023).

The average fracture densities controlled by mechanical stratigraphy exhibit a negative correlation with layer thickness, following either a linear relationship (Narr and Suppe, 1991; Gong

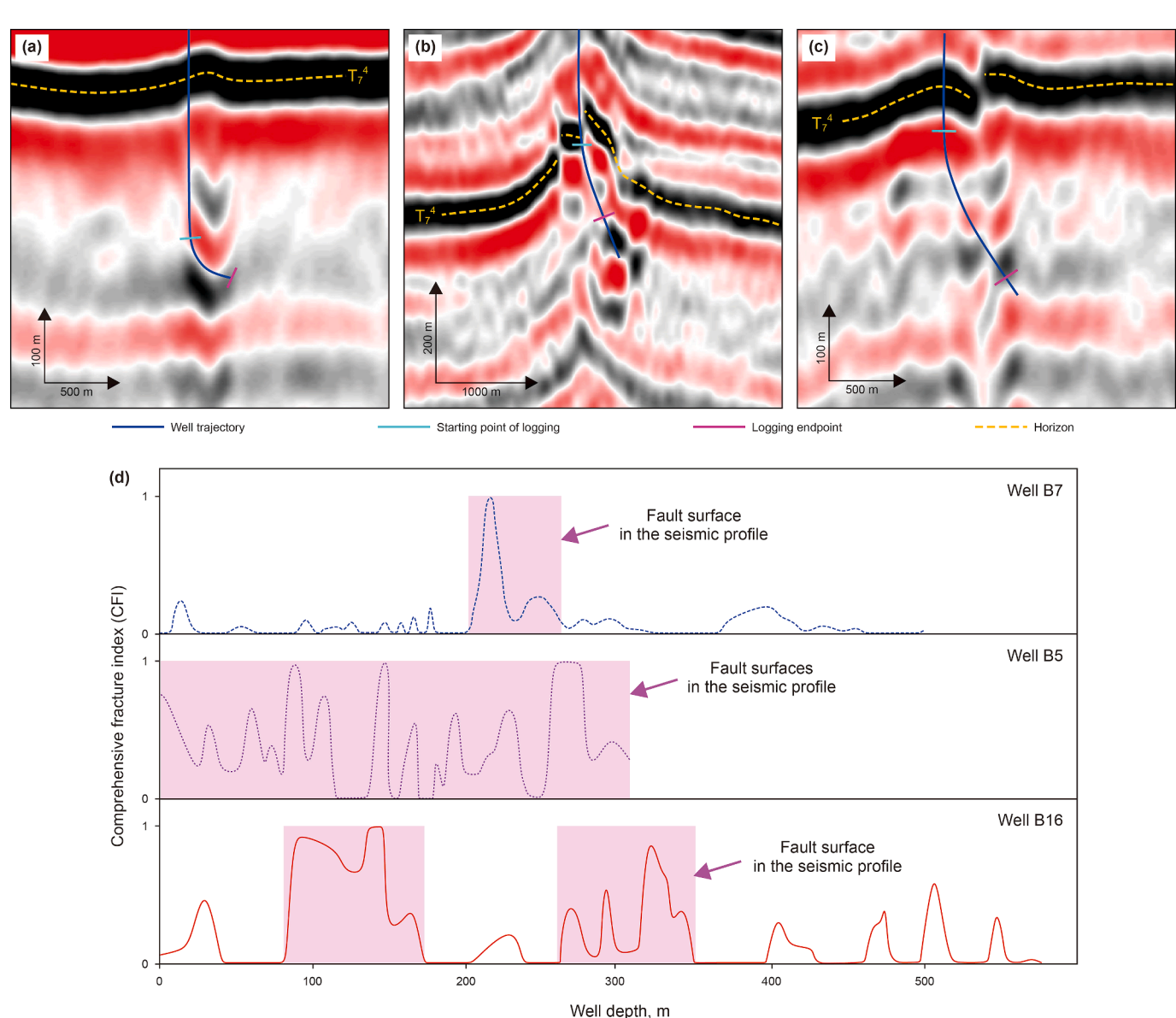


Fig. 14. Fracture development pattern and internal structure of strike-slip fault zones. (a) Well trajectory and seismic section of Well B7 in a non-stepover. (b) Well trajectory and seismic section of Well B5 in a transpressional stepover. (c) Well trajectory and seismic section of Well B16 in a transtensional stepover. (d) Fracture development zones predicted by the CFI method using well logging data. The prediction results show that the horizontal width of most fracture development zones does not exceed 100 m, and the fracture development zones are separated by tight wall rocks.

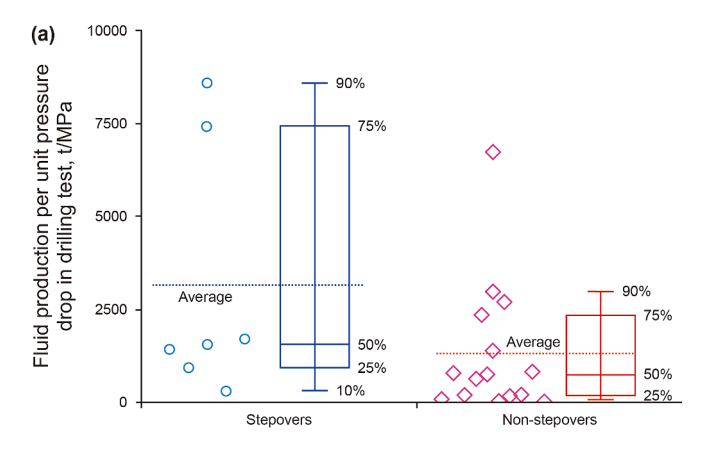
et al., 2018) or a power-law relationship (Ji et al., 2021). Both relationships indicate that thinner mechanical units have higher fracture densities. In the SLU, the structural styles of stepovers (including both transpressional and transtensional segments) influence the thickness of the Cambrian salt layer (Bian et al., 2022) and the vertical connectivity of fractures (Chen et al., 2022). Additionally, intraclastic grainstone and packstone formations within the Ordovician carbonate host rock sequences are particularly favorable for fracture development (Sun et al., 2023). Consequently, mechanical stratigraphy contributes to the vertical partitioning of fractured reservoirs, enhances connectivity with source rocks, and promotes a higher abundance of fractures. These factors collectively create favorable conditions for high petroleum production.

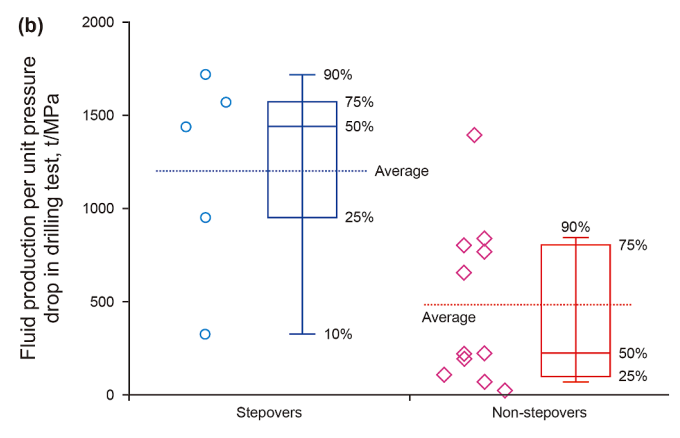
In summary, this study provides a quantitative characterization of fracture intensity, porosity, and dip angle within and adjacent to

a strike-slip fault system in ultradeep carbonates. It is important to accurately determine the dip angle of faults and fractures for subsurface reservoir modeling, drilling design, and seismic-based structural interpretation. The characteristics of natural fractures controlled by underground faults and the controlling factors on borehole productivity studied in this research provide valuable insights for optimizing the development of ultradeep fractured reservoirs controlled by strike-slip faults. Furthermore, this work also sheds light on strategies for future quantitative studies of insitu fracture density and dip angle in petroleum reservoirs.

6. Conclusions

1. Tectonic fractures dominate the ultradeep carbonate reservoirs in the central and northern Tarim Basin, substantially outnumbering fractures controlled by fluid overpressure and





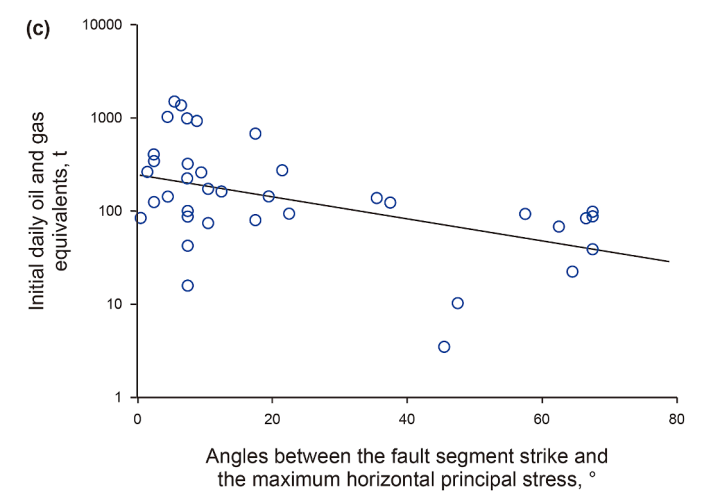


Fig. 15. Influence of structural styles and present-day stress field on fluid activity. (a) Liquid production per unit pressure drop of strike-slip fault stepovers and non-stepovers. The average liquid production of the fault stepovers (4575 t/MPa) is more than three times that of the non-stepovers (1340 t/MPa). (b) Liquid production less than 2000 t/MPa in (a). The average liquid production of the stepovers (1199 t/MPa) is about 2.5 times that of the non-stepovers (479 t/MPa). More than half of the wells in the non-stepovers produced less than the minimum value in the fault stepovers. (c) Relationship between the angle of a fault segment strike with the maximum horizontal principal compressive stress direction and reservoir production. The initial yield shows a decreasing trend as the angle increases.

- stylolites. These tectonic fractures play a critical role in controlling reservoir productivity.
- 2. The quantitative characterization of fault–fracture systems across and along the strike of a strike-slip fault zone, as well as perpendicular to bedding, provides a more accurate

- representation of the structural architecture of fault zones. Strike-slip faults strongly control the heterogeneity of natural fracture development, particularly in terms of intensity and dip angle. P_{21} , P_{22} , and fracture aperture decrease with the increasing distance from the PDZ. Tectonic fractures are more extensively developed in strike-slip fault stepovers than in non-stepovers, with fracture intensity in the central stepover considerably higher than at its two ends.
- 3. The development of stepovers and the direction of present-day in-situ stresses are key factors that control the productivity of fractured reservoirs controlled by strike-slip faults. The fault damage zone in the stepover shows a larger volume of fractured rocks and a higher density of faults and fractures, making them highly promising targets for petroleum exploration. Determining the dip angle of faults and fractures provides valuable guidance for selecting favorable exploration targets.

CRediT authorship contribution statement

Dong-Sheng Cao: Writing – original draft, Software, Resources, Investigation, Formal analysis. Jun Han: Visualization, Resources. Lian-Bo Zeng: Project administration, Investigation, Funding acquisition, Formal analysis, Data curation, Conceptualization. Cheng Huang: Visualization, Resources. Paul Dirk Bons: Writing – review & editing. Guo-Ping Liu: Writing – original draft, Visualization, Validation, Resources, Investigation. Ying-Tao Yao: Resources, Investigation. Wen-Ya Lyu: Resources, Investigation. Isaac Naaman: Writing – review & editing. Ling-Ping Zeng: Investigation.

Declaration of competing interest

The authors declare that they have no known competing financial interests or personal relationships that could have appeared to influence the work reported in this paper.

Acknowledgements

This research was supported by the National Natural Science Foundation of China (No. U21B2062). The first author acknowledges funding from the Chinese Scholarship Council (CSC) and the American Association of Petroleum Geologists Foundation Grantsin-Aid Program. The authors thank the oilfield engineers for their guidance and assistance in project research. The authors also thank the editor and several anonymous reviewers for their constructive comments.

References

Agosta, F., Tondi, E., 2010. Faulting and fracturing of carbonate rocks: new insights into deformation mechanisms, petrophysics and fluid flow properties. J. Struct. Geol. 9 (32), 1185–1186. https://doi.org/10.1016/j.jsg.2010.04.008.

Bian, Q., Deng, S., Lin, H.X., Han, J., 2022. Strike-slip salt tectonics in the Shuntuoguole low Uplift, Tarim Basin, and the significance to petroleum exploration. Mar. Petrol. Geol. 139, 105600. https://doi.org/10.1016/j.marpetgeo.2022.105600.

Bisdom, K., Gauthier, B.D.M., Bertotti, G., Hardebol, N.J., 2014. Calibrating discrete fracture-network models with a carbonate three-dimensional outcrop fracture network: implications for naturally fractured reservoir modeling. AAPG Bull. 98 (7), 1351–1376. https://doi.org/10.1306/02031413060.

Bons, P.D., Cao, D.S., de Riese, T., González-Esvertit, E., Koehn, D., Naaman, I., Sachau, T., Tian, H., Gomez-Rivas, E., 2022. A review of natural hydrofractures in rocks. Geol. Mag. 1–26. https://doi.org/10.1017/S0016756822001042.

Bons, P.D., Elburg, M.A., Gomez-Rivas, E., 2012. A review of the formation of tectonic veins and their microstructures. J. Struct. Geol. 43, 33–62. https://doi.org/10.1016/j.jsg.2012.07.005.

Brock, W.G., Engelder, T., 1977. Deformation associated with the movement of the Muddy Mountain overthrust in the Buffington window, southeastern Nevada.

Geol. Soc. Am. Bull. 88 (11), 1667–1677. https://doi.org/10.1130/0016-7606 (1977)88<1667:DAWTMO>2.0.CO;2.

- Caine, J.S., Evans, J.P., Forster, C.B., 1996. Fault zone architecture and permeability structure. Geology 24 (11), 1025–1028. https://doi.org/10.1130/0091-7613 (1996)024<1025:FZAAPS>2.3.CO;2.
- Cao, D.S., Zeng, L.B., Gomez-Rivas, E., Gong, L., Liu, G.P., Lu, G.Q., Bons, D.P., 2024. Correction of linear fracture density and error analysis using underground borehole data. J. Struct. Geol. 184, 105152. https://doi.org/10.1016/j. jsg.2024.105152.
- Cao, D.S., Zeng, L.B., Huang, C., Han, J., Gong, L., Song, Y.C., Yao, Y.T., Dong, S.Q., 2023. Control of multi-scale mechanical stratigraphy on development of faults and fractures. Earth Sci. 48 (7), 2535–2556. https://doi.org/10.3799/dqkx.2022.498 (in Chinese).
- Chai, Z., Chen, Z.H., Liu, H., Cao, Z.C., Cheng, B., Wu, Z.P., Qu, J.G., 2020. Light hydrocarbons and diamondoids of light oils in deep reservoirs of Shuntuoguole Low Uplift, Tarim Basin: implication for the evaluation on thermal maturity, secondary alteration and source characteristics. Mar. Petrol. Geol. 117, 104388. https://doi.org/10.1016/j.marpetgeo.2020.104388.
- Chen, J.J., He, D.F., Tian, F.L., Huang, C., Ma, D.B., Zhang, W.K., 2022. Control of mechanical stratigraphy on the stratified style of strike-slip faults in the central Tarim Craton, NW China. Tectonophysics 830, 229307. https://doi.org/10.1016/j.tecto.2022.229307
- Choi, J.H., Edwards, P., Ko, K., Kim, Y.S., 2016. Definition and classification of fault damage zones: a review and a new methodological approach. Earth Sci. Rev. 152, 70–87. https://doi.org/10.1016/j.earscirev.2015.11.006.
- 152, 70–87. https://doi.org/10.1016/j.earscirev.2015.11.006.

 Cunningham, W.D., Mann, P., 2007. Tectonics of strike-slip restraining and releasing bends. In: Geological Society, vol. 290. Special Publications, London, pp. 1–121. https://doi.org/10.1144/SP290.1.
- Deng, S., Liu, Y., Liu, J., Han, J., Wang, B., Zhao, R., 2021. Structural styles and evolution models of intracratonic strike-slip faults and the implications for reservoir exploration and appraisal: a case study of the Shunbei Area, Tarim Basin. Geotect. Metallogenia. 45 (6), 1111–1126. https://doi.org/10.16539/j.ddgzyckx.2020.05.015 (in Chinese).
- Dershowitz, W.S., Herda, H.H., 1992. Interpretation of fracture spacing and intensity. In: The 33rd US Symposium on Rock Mechanics (USRMS). OnePetro, pp. 757–766.
- Dooley, T.P., Schreurs, G., 2012. Analogue modelling of intraplate strike-slip tectonics: a review and new experimental results. Tectonophysics 574, 1–71. https://doi.org/10.1016/j.tecto.2012.05.030.
- Dooley, T., McClay, K., 1997. Analog modeling of pull-apart basins. AAPG Bull. 81 (11), 1804–1826. https://doi.org/10.1306/3B05C636-172A-11D7-8645000102C1865D.
- Dooley, T., McClay, K., Bonora, M., 1999. 4D evolution of segmented strike-slip fault systems: applications to NW Europe. Geological Society, London, Petroleum Geology Conference series: Geological Society of London 5 (1), 215–225. https://doi.org/10.1144/0050215.
- Du, Y.N., Wu, K.Y., Liu, Y., Li, Y.Y., Cao, Z.C., Cui, Y.W., Liu, J., 2024. Geometry and formation mechanism of tension gashes and their implication on the hydrocarbon accumulation in the deep-seated strata of sedimentary basin: a case from Shunnan area of Tarim Basin. Pet. Sci. 21, 87–99. https://doi.org/10.1016/j.petsci.2023.10.021.
- Faulkner, D.R., Jackson, C.A.L., Lunn, R.J., Schlische, R.W., Shipton, Z.K., Wibberley, C. A.J., Withjack, M.O., 2010. A review of recent developments concerning the structure, mechanics and fluid flow properties of fault zones. J. Struct. Geol. 32 (11), 1557–1575. https://doi.org/10.1016/j.jsg.2010.06.009.
- Faulkner, D.R., Mitchell, T.M., Jensen, E., et al., 2011. Scaling of fault damage zones with displacement and the implications for fault growth processes. J. Geophys. S Res.-Sol. Ea. 116, B05403. https://doi.org/10.1029/2010JB007788.
- Gomez-Rivas, E., Martín-Martín, J.D., Bons, P.D., Koehn, D., Griera, A., Travé, A., Llorens, M.G., Humphrey, E., Neilson, J., 2022. Stylolites and stylolite networks as primary cotrols on the geometry and distribution of carbonate diagenetic distributions. Mar. Petrol. Geol. 136, 105444. https://doi.org/10.1016/j. marpetgeo.2021.105444.
- Gong, L., Yao, J.Q., Gao, S., Wei, B., Zeng, L.B., Fu, X.F., Gao, Z.Y., Zu, K.W., Tian, H., 2018. Controls of rock mechanical stratigraphy on tectonic fracture spacing. Geotect. Metallogenia 42 (6), 965–973. https://doi.org/10.16539/j.ddgzyckx.2018.06.002 (in Chinese).
- He, B., Liu, Y.C., Qiu, C., Liu, Y., Su, C., Tang, Q.S., Tian, W.Z., Wu, G.H., 2023. The strike-slip fault effects on the Ediacaran carbonate tight reservoirs in the central Sichuan Basin, China. Energies 16 (10), 4041. https://doi.org/10.3390/en16104041.
- He, J.M., Wang, X.Y., Sun, J.F., Sun, X.T., Shi, J.X., Cao, D.S., Zeng, L.B., 2019. Characteristics and main controlling factors of natural fractures in the Lower-to-Middle Ordovician carbonate reservoirs in Tahe area, Northern Tarim Basin. Oil Gas Geol. 40 (5), 1022–1030. https://doi.org/10.11743/ogg20190507 (in Chinese).
- He, Z.L., Jin, X.H., Wo, Y.J., Li, H.L., Bai, Z.R., Jiao, C.L., Zhang, Z.P., 2016. Hydrocarbon accumulation characteristics and exploration domains of ultra-deep marine carbonates in China. China Petroleum Exploration 21 (1), 3–14. https://doi.org/10.3969/j.issn.1672-7703.2016.01.001 (in Chinese).
 Healy, D., Rizzo, R.E., Cornwell, D.G., Farrell, N.J.C., Watkins, H., Timms, N.E.,
- Healy, D., Rizzo, R.E., Cornwell, D.G., Farrell, N.J.C., Watkins, H., Timms, N.E., Gomez-Rivas, E., Smith, M., 2017. FracPaQ: a MATLAB™ toolbox for the quantification of fracture patterns. J. Struct. Geol. 95, 1–16. https://doi.org/10.1016/j. jsg.2016.12.003.

Heap, M., Reuschlé, T., Baud, P., Renard, F., lezzi, G., 2018. The permeability of stylolite-bearing limestone. J. Struct. Geol. 116, 81–93. https://doi.org/10.1016/j.isg.2018.08.007.

- Hennings, P., Allwardt, P., Paul, P., Zahm, C., Reid, Jr R., Alley, H., Kirschner, R., Lee, B., Hough, E., 2012. Relationship between fractures, fault zones, stress, and reservoir productivity in the Suban gas field, Sumatra, Indonesia Suban Gas Field, Sumatra, Indonesia. AAPG Bull. 96 (4), 753–772. https://doi.org/10.1306/ 08161109084
- Huang, C., 2019. Multi-stage activity characteristics of small-scale strike-slip faults in superimposed basin and its identification method: a case study of Shunbei area, Tarim Basin. Petroleum Geology & Experiment 41 (3), 379–389. https:// doi.org/10.11781/sysyd2201903379 (in Chinese).
- Ingebritsen, S.E., Manning, C.E., 1999. Geological implications of a permeability-depth curve for the continental crust. Geology 27 (12), 1107–1110. https://doi.org/10.1130/0091-7613(1999)027<1107:GIOAPD>2.3.CO;2.
- Ji, S.C., Li, L., Marcotte, D., 2021. Power-law relationship between joint spacing and bed thickness in sedimentary rocks and implications for layered rock mechanics. J. Struct. Geol. 150, 104413. https://doi.org/10.1016/j.jsg.2021.104413.
- Jia, C.Z., Ma, D.B., Yuan, J.Y., Wei, G.Q., Yang, M., Yan, L., Tian, F.L., Jiang, L., 2022. Structural characteristics, formation & evolution and genetic mechanisms of strizke-slip faults in the Tarim Basin. Nat. Gas. Ind. 9 (1), 51–62. https://doi.org/ 10.1016/j.ngib.2021.08.017.
- Jia, C.Z., Wei, G.Q., 2002. Structural characteristics and petroliferous features of Tarim Basin. Chin. Sci. Bull. 47, 1–11. https://doi.org/10.1007/BF02902812.
- Jia, C.Z., 1999. Structural characteristics and oil/gas accumulative regularity in Tarim Basin. Xinjing Pet. Geol. 20 (3), 177–183. https://doi.org/10.3969/j. issn.1001-3873.1999.03.001 (in Chinese).
- Jiao, F.Z., 2017. Significance of oil and gas exploration in NE strike-slip fault belts in Shuntuoguole area of Tarim Basin. Oil Gas Geol. 38 (5), 831–839. https://doi. org/10.11743/ogg20170501 (in Chinese).
- Jiao, F.Z., 2018. Significance and prospect of ultra-deep carbonate fault-karst reservoirs in Shunbei area, Tarim Basin. Oil Gas Geol. 39 (2), 207–216. https://doi.org/10.11743/ogg20180201 (in Chinese).
- org/10.11743/ogg20180201 (in Chinese).

 Johri, M., Zoback, M.D., Hennings, P., 2014. A scaling law to characterize fault-damage zones at reservoir depths. AAPG Bull. 98 (10), 2057–2079. https://doi.org/10.1306/05061413173.
- Koehn, D., Rood, M.P., Beaudoin, N., Chung, P., Bons, P.D., Gomez-Rivas, E., 2016. A new stylolite classification scheme to estimate compaction and local permeability variations. Sediment. Geol. 346, 60–71. https://doi.org/10.1016/j. sedgeo.2016.10.007.
- Kuang, A.P., Cao, D.S., Zeng, L.B., Huang, C., Yao, Y.T., Han, J., 2021. Drilling and logging identification of the ultra-deep carbonate fault-karst reservoirs in Shunbei area of Tarim basin. Petroleum geology and engineering 35 (3), 35–40. https://doi.org/10.3969/j.issn.1673-8217.2021.03.007 (in Chinese).
- Laubach, S.E., Olson, J.E., Gross, M.R., 2009. Mechanical and fracture stratigraphy. AAPG Bull. 93 (11), 1413–1426. https://doi.org/10.1306/07270909094.
- Laubach, S.E., Zeng, L., Hooker, J.N., Wang, Q.Q., Zhang, R.H., Wang, J.P., Ren, B., 2023. Deep and ultra-deep basin brittle deformation with focus on China. J. Struct. Geol. 175, 104938. https://doi.org/10.1016/j.jsg.2023.104938.
- Lin, B., Yun, L., Zhang, X., Xiao, C.Y., Kuang, A.P., Xu, X.C., Cao, Z.C., 2021. A method for plane segmentation of small-scale intraplate strike-slip faults: a case of the middle-north segment of Shunbei No. 5 Fault in Tarim Bassin. Journal of Jilin University, Earth Science Edition 51 (4), 1006–1018. https://doi.org/10.13278/j. cnki.jjuese.20200122 (in Chinese).
- Liu, B., 2020. Analysis of main controlling factors of oil and gas differential accumulation in Shunbei area, Tarim Basin: taking Shunbei No.1 and No.5 strike slip fault zones as examples. China Petroleum Exploration 25 (3), 83–95. https://doi.org/10.3969/j.issn.1672-7703.2020.03.008, 2020 (in Chinese).
- Liu, P.X., Deng, S.B., Guan, P., Jin, Y.Q., Wang, K., Chen, Y.Q., 2020a. The nature, type, and origin of diagenetic fluids and their control on the evolving porosity of the Lower Cambrian Xiaoerbulak Formation dolostone, northwestern Tarim Basin, China. Pet. Sci. 17, 873–895. https://doi.org/10.1007/s12182-020-00434-0.
- Liu, G.P., Zeng, L.B., Wang, X.J., Ostadhassan, M., Wang, Z.L., Mao, Z., Tie, Q., 2020b. Natural fractures in deep tight gas sandstone reservoirs in the thrust belt of the southern Junggar Basin, northwestern China. Interpretation 8 (4), 81–93. https://doi.org/10.1190/INT-2020-0051.1.
- Lorenz, J.C., Cooper, S.P., 2017. Atlas of Natural and Induced Fractures in Core. John Wiley & Sons.
- Lorenz, J.C., Cooper, S.P., 2020. Applied Concepts in Fractured Reservoirs. John Wiley & Sons.
- Lorenz, J.C., Cooper, S.P., Olsson, W.A., 2006. Natural fracture distributions in sinuous, channel-fill sandstones of the Cedar Mountain Formation, Utah. AAPG Bull. 90 (9), 1293–1308. https://doi.org/10.1306/03300605137.
- Lyu, W.Y., Zeng, L.B., Chen, S.Q., Lyu, P., Dong, S.Q., Hui, C., Li, R.Q., Wang, H.N., 2021. Characterization methods of multi-scale natural fractures in tight and low-permeability sandstone reservoirs. Geol. Rev. 67 (2), 543–556 (in Chinese). doi:10.16509/j.georeview.2021.02.020.
- Lyu, W.Y., Zeng, L.B., Liao, Z.H., Ji, Y.Y., Lyu, P., Dong, S.Q., 2017. Fault damage zone characterization in tight-oil sandstones of the Upper Triassic Yanchang Formation in the southwest Ordos Basin, China: integrating cores, image logs, and conventional logs. Interpretation 5 (4), 27–39. https://doi.org/10.1190/INT-2016-02311
- Ma, D.B., Wu, G.H., Scarselli, N., Luo, X.S., Han, J.F., Chen, Z.Y., 2019. Seismic damage zone and width-throw scaling along the strike-slip faults in the Ordovician

carbonates in the Tarim Basin. Pet. Sci. 16, 752–762. https://doi.org/10.1007/s12182-019-0352-4

- Ma, Q.Y., Cao, Z.C., Jiang, H.S., Lan, M.J., 2020. Source-connectivity of strike-slip fault zone and its relationship with oil and gas accumulation in Tahe-Shunbei area, Tarim Basin. Marine Origin Petroleum Geology 25 (4), 327–334. https://doi.org/10.3969/j.issn.1672-9854.2020.04.005 (in Chinese).
- Ma, Y.S., Cai, X.Y., Yun, L., Li, Z.J., Li, H.L., Deng, S., Zhao, P.R., 2022. Practice and theoretical and technical progress in exploration and development of Shunbei ultra-deep carbonate oil and gas field, Tarim Basin, NW China. Petrol. Explor. Dev. 49 (1), 1–20. https://doi.org/10.1016/S1876-3804(22)60001-6.
- Mann, P., 2007. Global catalogue, classification and tectonic origins of restrainingand releasing bends on active and ancient strike-slip fault systems. In: Geological Society, vol. 290. Special Publications, London, pp. 13–142. https:// doi.org/10.1144/SP290.2.
- Meng, Y.J., Chen, H.H., Luo, Y., Zhao, Y.C., Tang, D.Q., He, F.Q., 2023. Architecture of intraplate strike-slip fault zones in the Yanchang Formation, Southern Ordos Basin, China: characterization and implications for their control on hydrocarbon enrichment. J. Struct. Geol. 170, 104851. https://doi.org/10.1016/j. iss.2023.104851.
- Nabavi, S.T., Alavi, S.A., Mohammadi, S., Ghassemi, M.R., Frehner, M., 2017. Analysis of transpression within contractional fault steps using finite-element method. J. Struct. Geol. 96, 1–20. https://doi.org/10.1016/j.jsg.2017.01.004.
- Narr, W., Suppe, J., 1991. Joint spacing in sedimentary rocks. J. Struct. Geol. 13 (9), 1037–1048. https://doi.org/10.1016/0191-8141(91)90055-N.
- Nelson, R.A., 2001. Geologic Analysis of Naturally Fractured Reservoirs. Elsevier. Nelson, R.A., 2019. Static Conceptual Fracture Modeling: Preparing for Simulation and Development. John Wiley & Sons.
- Ogata, K., Storti, F., Balsamo, F., Tinterri, R., Bedogni, E., Fetter, M., Gomes, L., Hatushika, R., 2017. Sedimentary facies control on mechanical and fracture stratigraphy in turbidites. Geol. Soc. Am. Bull. 129 (1–2), 76–92. https://doi.org/10.1130/B315171
- Ortega, O.J., Marrett, R.A., Laubach, S.E., 2006. A scale-independent approach to fracture intensity and average spacing measurement. AAPG Bull. 90 (2), 193–208. https://doi.org/10.1306/08250505059.
- Pang, X.Q., Tian, J., Pang, H., Xiang, C.F., Jiang, Z.X., Li, S.M., 2010. Main progress and problems in research on Ordovician hydrocarbon accumulation in the Tarim Basin. Pet. Sci. 7, 147–163. https://doi.org/10.1007/s12182-010-0022-z.
- Peacock, D.C.P., 2006. Predicting variability in joint frequencies from boreholes. J. Struct. Geol. 28 (2), 353–361. https://doi.org/10.1016/j.jsg.2005.10.007.
- Qi, L.X., 2020. Characteristics and inspiration of ultra-deep fault-karst reservoir in the Shunbei area of the Tarim Basin. China Petroleum Exploration 25 (1), 106–115. https://doi.org/10.3969/j.issn.1672-7703.2020.01.010 (in Chinese).
- Rashid, F., Hussein, D., Lawrence, J.A., Khanaqa, P., 2020. Characterization and impact on reservoir quality of fractures in the Cretaceous Qamchuqa Formation, Zagros folded belt. Mar. Petrol. Geol. 113, 104117. https://doi.org/10.1016/j. marpetgeo.2019.104117.
- Sanderson, D.J., Nixon, C.W., 2015. The use of topology in fracture network characterization. J. Struct. Geol. 72, 55–66. https://doi.org/10.1016/j.jsg.2015.01.005.
- Savage, H.M., Brodsky, E.E., 2011. Collateral damage: evolution with displacement of fracture distribution and secondary fault strands in fault damage zones. J. Geophys.S Res.Sol. Ea. 116, B03405. https://doi.org/10.1029/2010JB007665.
- Schellart, W.P., Nieuwland, D.A., 2003. 3D evolution of a pop-up structure above a double basement strike-slip fault: some insights from analogue modelling. In: Geological Society, 212. Special Publications, London, pp. 169–179. https://doi. org/10.1144/GSL.SP.2003.212.01.11.
- Smeraglia, L., Fabbi, S., Billi, A., Carminati, E., Cavinato, G.P., 2022a. How hydrocarbons move along faults: evidence from microstructural observations of hydrocarbon-bearing carbonate fault rocks. Earth Planet Sci. Lett. 584, 117454. https://doi.org/10.1016/j.epsl.2022.117454.
- Smeraglia, L., Fabbi, S., Maffucci, R., Albanesi, L., Carminati, E., Billi, A., Cavinato, G. P., 2022b. The role of post-orogenic normal faulting in hydrocarbon migration in foldand-thrust belts: insights from the central Apennines, Italy. Mar. Petrol. Geol. 136, 105429. https://doi.org/10.1016/j.marpetgeo.2021.105429.
- Su, J., Wang, Y., Wang, X.N., He, K., Yang, H.J., Wang, H.T., Wang, H.J., Zhang, B., Huang, L., Weng, N., Bi, L.N., Xiao, Z.H., 2017. Impact of formation water on the generation of H₂S in condensate reservoirs: a case study from the deep Ordovician in the Tazhong Uplift of the Tarim Basin, NW China. Pet. Sci. 14, 507–519. https://doi.org/10.1007/s12182-017-0176-z.
- Sun, Q., Fan, T., Gao, Z., Wu, J., Zhang, H.H., Jiang, Q., Liu, N., Yuan, Y.Y., 2021. New insights on the geometry and kinematics of the Shunbei 5 strike-slip fault in the central Tarim Basin, China. J. Struct. Geol. 150, 104400. https://doi.org/ 10.1016/j.jsg.2021.104400.
- Sun, Q.Q., Fan, T.L., Holdsworth, R.E., Gao, Z.Q., Wu, J., Gao, S.C., Wang, M., Yuan, Y. X., 2023. The spatial characterization of stepovers along deeply-buried strike-slip faults and their influence on reservoir distribution in the central Tarim Basin, NW China. J. Struct. Geol. 170, 104849. https://doi.org/10.1016/j.jsg.2023.104849.
- Sylvester, A.G., 1988. Strike-slip faults. Geol. Soc. Am. Bull. 100 (11), 1666–1703. https://doi.org/10.1130/0016-7606(1988)100<1666:SSF>2.3.CO;2.
- Tchalenko, J.S., 1970. Similarities between shear zones of different magnitudes. Geol. Soc. Am. Bull. 81 (6), 1625–1640. https://doi.org/10.1130/0016-7606 (1970)81[1625:SBSZOD]2.0.CO;2.
- Teng, C.Y., Cai, Z.X., Hao, F., Cao, Z.C., 2020. Structural geometry and evolution of an intracratonic strike-slip fault zone: a case study from the north SB5 fault zone

- in the Tarim Basin, China. J. Struct. Geol. 140, 104159. https://doi.org/10.1016/j.jsg.2020.104159.
- Terzaghi, R.D., 1965. Sources of error in joint surveys. Geotechnique 15 (3), 287–304. https://doi.org/10.1680/geot.1965.15.3.287.
- van Der Voet, E., Muchez, P., Laenen, B., Weltje, G.J., Lagrou, D., Swennen, R., 2020. Characterizing carbonate reservoir fracturing from borehole data-a case study of the Viséan in northern Belgium. Mar. Petrol. Geol. 111, 375–389. https://doi.org/10.1016/j.marpetgeo.2019.08.040.
- Wang, J., Xie, H.P., Matthai, S.K., Hu, J.J., Li, C.B., 2023. The role of natural fracture activation in hydraulic fracturing for deep unconventional geo-energy reservoir stimulation. Pet. Sci. 20, 2141–2164. https://doi.org/10.1016/j. petsci.2023.01.007.
- Wang, Q.H., Yang, H.J., Li, Y., Lyu, X.X., Zhang, Y.T., Zhang, Y.Q., Sun, C., Ouyang, S.Q., 2022a. Control of strike-slip fault on the large carbonate reservoir in Fuman, Tarim Basin—a reservoir model. Earth Sci. Front. 29 (6), 239–251. https://doi.org/10.13745/j.esf.sf.2022.8.17 (in Chinese).
- Wang, W.Y., Pang, X.Q., Wang, Y.P., Chen, Z.X., Jiang, F.J., Chen, Y., 2024. Quantitative prediction model for the depth limit of oil accumulation in the deep carbonate rocks: a case study of Lower Ordovician in Tazhong area of Tarim Basin. Pet. Sci. 21, 115–124. https://doi.org/10.1016/j.petsci.2023.11.013.
 Wang, Z.Z., Gao, Z.Q., Fan, T.L., Shang, Y.X., Qi, L.X., Yun, L., 2020. Structural char-
- Wang, Z.Z., Gao, Z.Q., Fan, T.L., Shang, Y.X., Qi, L.X., Yun, L., 2020. Structural characterization and hydrocarbon prediction for the SB5M strike-slip fault zone in the Shuntuo Low Uplift, Tarim Basin. Mar. Petrol. Geol. 117, 104418. https://doi.org/10.1016/j.marpetgeo.2020.104418.
- Wang, Z.Y., Gao, Z.Q., Fan, T.L., Zhang, H.H., Yuan, Y.X., Wei, D., Qi, L.X., Yun, L., Karubandika, G.M., 2022b. Architecture of strike-slip fault zones in the central Tarim Basin and implications for their control on petroleum systems. J. Petrol. Sci. Eng. 213, 110432. https://doi.org/10.1016/j.petrol.2022.110432.
- Wennberg, O.P., Casini, G., Jonoud, S., Peacock, D.C.P., 2016. The characteristics of open fractures in carbonate reservoirs and their impact on fluid flow: a discussion. Pet. Geosci. 22 (1), 91–104. https://doi.org/10.1144/petgeo2015-003.
- Wu, G.H., Kim, Y.S., Su, Z., Yang, P.F., Ma, D.B., Zheng, D.M., 2020. Segment interaction and linkage evolution in a conjugate strike-slip fault system from the Tarim Basin, NW China. Mar. Petrol. Geol. 112, 104054. https://doi.org/10.1016/j.marpetgeo.2019.104054.
- Wu, G.H., Ma, B.S., Han, J.F., Guan, B.H., Chen, X., Yang, P., Xie, Z., 2021. Origin and growth mechanisms of strike-slip faults in the central Tarim cratonic basin, NW China. Petrol. Explor. Dev. 48 (3), 595–607. https://doi.org/10.1016/S1876-3804(21)60048-4.
- Wu, J.Z., Shi, Y., Wang, W.H., 2022. Fault imaging of seismic data based on a modified u-net with dilated convolution. Appl. Sci. 12 (5), 2451. https://doi.org/ 10.3390/app12052451.
- Yang, P., Wu, G.H., Ren, Z.L., Zhou, R.J., Zhao, J.X., Zhang, L.P., 2020a. Tectonothermal evolution of Cambrian-Ordovician source rocks and implications for hydrocarbon generation in the eastern Tarim Basin, NW China. J. Asian Earth Sci. 194, 104267. https://doi.org/10.1016/j.jseaes.2020.104267.
- Yang, H.J., Deng, X.L., Zhang, Y.T., Xie, Z., Li, Y., Li, S.Y., Zhang, H.Z., Zhu, Y.F., Chen, Y. Q., 2020b. Great discovery and its significance of exploration for Ordovician ultra-deep fault-controlled carbonate reservoirs of Well Manshen 1 in Tarim Basin. China Petroleum Exploration 25 (3), 13–23. https://doi.org/10.3969/J. ISSN.1672-7703.2020.03.002 (in Chinese).
- Yang, P., Wu, G.H., Nuriel, P., Nguyen, A.D., Chen, Y.Q., Yang, S., Feng, Y.X., Ren, Z.L., Zhao, J.X., 2021a. In situ LA-ICPMS U-Pb dating and geochemical characterization of fault-zone calcite in the central Tarim Basin, northwest China: implications for fluid circulation and fault reactivation. Chem. Geol. 568, 120125. https://doi.org/10.1016/j.chemgeo.2021.120125.
- Yang, P., Liu, K.Y., Liu, J.L., Yu, S., Yu, B., Hou, M.G., Wu, L.Y., 2021b. Petroleum charge history of deeply buried carbonate reservoirs in the Shuntuoguole Low Uplift, Tarim Basin. west China. Mar. Petrol. Geol. 128, 105063. https://doi.org/ 10.1016/j.marpetgeo.2021.105063.
- Yang, R.Q., 2021. Numerical Simulation of In-Situ Stress Fields and Optimization of Borehole Trajectory in Shunbei No.5 Fault Zone. Master Thesis, China University of Geosciences (Beijing), Beijing, pp. 34–37 (in Chinese). https://doi.org/10. 1007/s12182-019-00360-w.
- Yang, X.F., Lin, C.S., Yang, H.J., Han, J.F., Liu, J.Y., Zhang, Y.M., Peng, L., Jing, B., Tong, J. Y., Wang, H.P., Li, H.P., 2010. Depositional architecture of the late Ordovician drowned carbonate platform margin and its responses to sea-level fluctuation in the northern slope of the Tazhong region, Tarim Basin. Pet. Sci. 7, 323–336. https://doi.org/10.1007/s12182-010-0074-0.
- Yang, P., Ren, Z.L., Fu, J.H., Bao, H.P., Xiao, H., Shi, Z., Wang, K., Zhang, Y.Y., Liu, W.H., Li, W.H., 2024a. A tectono-thermal perspective on the petroleum generation, accumulation and preservation in the southern Ordos Basin, North China. Pet. Sci. 21 (3), 1459–1473. https://doi.org/10.1016/j.petsci.2023.12.006.
- Yang, P., Ren, Z.L., Nuriel, P., Nguyen, A.D., Feng, Y.X., Zhou, R.J., Zhao, J.X., 2024b. Cenozoic faulting leading to petroleum escape in SW Ordos Basin, China: evidence from fault-related calcite in situ U-Pb dating, rare earth elements and fluid inclusions. Mar. Petrol. Geol. 170, 107071. https://doi.org/10.1016/j.marpetgeo.2024.107071.
- Yao, Y.T., Zeng, L.B., Dong, S.Q., Huang, C., Cao, D.S., Mao, Z., Kuang, A.P., Lyu, W.Y., 2024. Using seismic methods to detect connectivity of fracture networks controlled by strike-slip faults in ultra-deep carbonate reservoirs: a case study in northern Tarim Basin, China. J. Struct. Geol. 180, 105060. https://doi.org/ 10.1016/j.jsg.2024.105060.

- Yao, Y.T., Zeng, L.B., Mao, Z., Han, J., Cao, D.S., Lin, B., 2023. Differential deformation of a strike-slip fault in the Paleozoic carbonate reservoirs of the Tarim Basin, China. J. Struct. Geol. 2023, 104908. https://doi.org/10.1016/j.jsg.2023.104908.
- Yun, L., 2021. Controlling effect of NE strike-slip fault system on reservoir development and hydrocarbon accumulation in the eastern Shunbei area and its geological significance, Tarim Basin. China Petroleum Exploration 26 (3), 41–52 (in Chinese). doi:10.3969/j.issn.1672-7703.2021.03.004.
- Yun, L., Cao, Z.C., 2014. Hydrocarbon enrichment pattern and exploration potential of the Ordovician in Shunnan area, Tarim Basin. Oil Gas Geol. 35 (6), 788–797. https://doi.org/10.11743/ogg20140606 (in Chinese).
- Zeeb, C., Gomez-Rivas, E., Bons, P.D., Virgo, S., Blum, P., 2013. Fracture network evaluation program (FraNEP): a software for analyzing 2D fracture trace-line maps. Comput. Geosci.-UK 60, 11–22. https://doi.org/10.1016/j.cageo.2013.04.027.
- Zeng, L.B., Gong, L., Guan, C., Zhang, B.J., Wang, Q.Q., Zeng, Q., Lyu, W.Y., 2022. Natural fractures and their contribution to tight gas conglomerate reservoirs: a case study in the northwestern Sichuan Basin, Chinas. J. Petrol. Sci. Eng. 210, 110028. https://doi.org/10.1016/j.petrol.2021.110028.
- Zeng, L.B., Gong, L., Zhang, Y.Z., Dong, S.Q., Lyu, W.Y., 2023b. A review of the genesis, evolution, and prediction of natural fractures in deep tight sandstones of China. AAPG Bull. 107 (10), 1687–1721. https://doi.org/10.1306/07052322120.
- Zeng, L.B., Li, Y.G., 2010. Tectonic fractures in the tight gas sandstones of the upper Triassic Xujiahe formation in the western Sichuan basin, China. ACTA Geol. Sin-Engl. 84 (5), 1229–1238. https://doi.org/10.1111/j.1755-6724.2010.00293.x.
- Zeng, L.B., Lyu, W.Y., Li, J., Zhu, L.F., Weng, J.Q., Yue, F., Zu, K.W., 2016. Natural fractures and their influence on shale gas enrichment in Sichuan Basin, China. J. Nat. Gas Sci. Eng. 30, 1–9. https://doi.org/10.1016/j.jngse.2015.11.048.
- Zeng, L.B., Shi, J.X., Ma, Q.Y., Lyu, W.Y., Dong, S.Q., Cao, D.S., Wei, H.H., 2024a. Strike-slip fault control on karst in ultra-deep carbonates, Tarim Basin, China. AAPG Bull. 108 (2), 235–260. https://doi.org/10.1306/09212321161.

- Zeng, L.B., Mao, Z., Liu, G.P., Tian, H., Yao, Y.Y., Zu, K.W., Dong, S.Q., Ostadhassan, M., 2024b. Controls of strike-slip fault on fractures: insight from 3D discrete element simulation. Sci. China Earth Sci. 67 (1), 146–164. https://doi.org/10.1007/s11430-022-1142-4.
- Zeng, L.B., Song, Y.C., Liu, G.P., Tan, X.L., Xu, X.T., Yao, Y.T., Mao, Z., 2023a. Natural fractures in ultra-deep reservoirs of China: a review. J. Struct. Geol., 104954 https://doi.org/10.1016/j.jsg.2023.104954.
- Zeng, L.B., Tang, X.M., Jiang, J.W., Peng, Y.M., Yang, Y.L., Lyu, W.Y., 2015. Unreliable determination of in situ stress orientation by borehole breakouts in fractured tight reservoirs: a case study of the upper Eocene Hetaoyuan Formation in the Anpeng field, Nanxiang Basin, China. AAPG Bull. 99 (11), 1991–2003. https://doi.org/10.1306/06011513195.
- Zhang, K., Liu, X.F., Wang, D.B., Zheng, B., Chen, T.H., Wang, Q., Bai, H., Yao, E.D., Zhou, F.J., 2023a. A review of reservoir damage during hydraulic fracturing of deep and ultra-deep reservoirs. Pet. Sci. 21, 384–409. https://doi.org/10.1016/j. petsci.2023.11.017.
- Zhao, Z., Liu, J.T., Ding, W.L., Yang, R.Q., Zhao, G., 2021. Analysis of seismic damage zones: a case study of the ordovician formation in the shunbei 5 fault zone, Tarim Basin, China. J. Mar. Sci. Eng. 9, 630. https://doi.org/10.3390/jmse9060630.
- Zhou, Y., Yang, F.L., Ji, Y.L., Zhou, X.F., Zhang, C.H., 2020. Characteristics and controlling factors of dolomite karst reservoirs of the Sinian Dengying Formation, central Sichuan Basin, southwestern China. Precambr. Res. 343, 105708. https://doi.org/10.1016/j.precamres.2020.105708.
- Zhu, M.J., Wu, G.Z., Li, S.Z., Liu, Y.J., Wang, P.C., Guo, L.L., Zhao, Li, Chen, X.P., Song, T. H., 2024. An overview of structures associated with bends of strike-slip faults: focus on analogue and numerical models. Mar. Petrol. Geol. 167, 106983. https://doi.org/10.1016/j.marpetgeo.2024.106983.